The Complex Dielectric Constant of Pure and Sea Water from Microwave Satellite Observations

Thomas Meissner and Frank Wentz

Abstract—We provide a new fit for the microwave complex dielectric constant of water in the salinity range between 0 and 40 ppt using two Debye relaxation wavelengths. For pure water, the fit is based on laboratory measurements including supercooled water in the temperature range between $-20^{\circ}C$ and $+40^{\circ}C$ and for frequencies up to 500 GHz. For sea water, our fit is valid for temperatures between $-2^{\circ}C$ and $+29^{\circ}C$ and for frequencies up to at least 100 GHz. At low frequencies, our new model is a modified version of the Klein-Swift model. We compare the results of the new fit with various other models and provide a validation using an extensive SSM/I brightness temperature analysis.

Index Terms— Dielectric Constant of Pure and Sea Water, Permittivity, Ocean Surface Emissivity, Microwave Radiometers, SSM/I.

The authors are with Remote Sensing Systems, 438 First Street, Suite 200, Santa Rosa, CA 95401.

Email: meissner@remss.com, wentz@remss.com. URL: http://www.remss.com.

I. INTRODUCTION

A precise knowledge of the complex dielectric constant (permittivity) ε of water is essential for studying the radiative transfer of microwave radiation that is emitted by the ocean surface, transmitted through the Earth's atmosphere and received by passive microwave sensors. The dielectric constant, which is a function of frequency ν, water temperature T and salinity S, enters in two ways into the radiative transfer equations:

The specular ocean surface emissivity E_0 for polarization p (= vertical (v) or horizontal (h)) at Earth incidence angle (EIA) θ is determined by the Fresnel equations:

$$E_{0p} = 1 - \left|\rho_p\right|^2$$
$$\rho_v = \frac{\varepsilon\cos(\theta) - \sqrt{\varepsilon - \sin^2(\theta)}}{\varepsilon\cos(\theta) + \sqrt{\varepsilon - \sin^2(\theta)}} \qquad (1).$$
$$\rho_h = \frac{\cos(\theta) - \sqrt{\varepsilon - \sin^2(\theta)}}{\cos(\theta) + \sqrt{\varepsilon - \sin^2(\theta)}}$$

Using Rayleigh approximation, the absorption coefficient α_L [neper/cm] of radiation with wavelength λ [cm] by a liquid cloud of density ρ_L [g/cm^3] is given by:

$$\alpha_L = \frac{6\pi\rho_L}{\lambda\rho_0}\,\mathrm{Im}\left(\frac{1-\varepsilon}{2+\varepsilon}\right) \qquad (2),$$

where $\rho_0 \approx 1\,{}^{g}\!/_{cm^3}$ is the density of water.

In the first case, the ε refers to sea water with a surface temperature $T = T_S$. In the second case, the water is pure and $T = T_L$ is the temperature of the cloud.

Physical retrieval algorithms for environmental data records (EDRs), such as the sea surface temperature (SST), sea surface wind speed, columnar water vapor and columnar liquid cloud water are derived from a radiative transfer model (RTM), which computes the brightness temperatures that are measured by the satellite as a function of these EDRs. The RTM is based on a

model for the sea surface emissivity and the theory of microwave absorption in the Earth's atmosphere. The performance of the EDR algorithms depends on the accuracy of sea surface emissivity and therefore on the value of the dielectric constant ε. Moreover, the microwave absorption due to liquid cloud water depends directly on the dielectric constant of pure water through equation (2). As we shall see, this dependence is relatively weak for low – medium frequencies and not too cold temperatures, in the sense that most dielectric models in the literature will predict very close results for the cloud water absorption, even if they differ substantially in their predictions of surface emissivities. The differences between the model cloud absorption predictions increase at higher frequencies (above 100 GHz) and for supercooled clouds.

So far, microwave radiative transfer calculations have mainly used the dielectric model of Klein and Swift [1]. It fits the dielectric constant with a single Debye relaxation law [2]:

$$\varepsilon(T,S) = \varepsilon_\infty + \frac{\varepsilon_S(T,S) - \varepsilon_\infty}{1 + \left(i \frac{\nu}{\nu_R(T,S)} \right)^{1-\eta}} - i \frac{\sigma(T,S)}{(2\pi\varepsilon_0)\nu} \qquad (3).$$

Here, $i = \sqrt{-1}$, ν is the radiation frequency [in GHz], $\varepsilon_S(T,S)$ the static (zero frequency) dielectric constant, ε_∞ is the dielectric constant at infinite frequencies, which is constant in the Klein-Swift model, $\nu_R(T,S)$ the Debye relaxation wavelength [in GHz], η the Cole-Cole spread factor [3], which is set to zero in the Klein-Swift model, $\sigma(T,S)$ is the conductivity of water [in S/m] and ε_0 is the vacuum electric permittivity, which is determined by $\frac{1}{2\pi\varepsilon_0} = 17.97510 \frac{GHz\ m}{S}$. The model parameters ε_∞, $\varepsilon_S(T,S)$ and $\nu_R(T,S)$ were fitted using laboratory measurements of the dielectric constants by Lane and Saxton [4] and the measurements by Ho et al. [5, 6] at 1.43 GHz and 2.653 GHz. The Klein-Swift model is sufficiently accurate at very low frequencies but, as it has been shown by various authors [7, 8], it is get-

ting increasingly inaccurate as the frequency increases. Wentz [9-11] observed that using the Klein-Swift model above 10 GHz leads to various inconsistencies in retrieving SSM/I EDRs, especially to an abundance of negative cloud water retrievals over cold sea surfaces. An updated analysis for the dielectric constant of pure and sea water for frequencies up to 37 GHz was provided in [11]. It is very similar to the Klein-Swift model, with two exceptions. First, the measurements of Lane and Saxton of the salinity dependence of ν_R were excluded from the data, as they are inconsistent with other measurements. Second, [11] use a single Debye relaxation law with a finite spread factor $\eta = 0.012$ and a value of $\varepsilon_\infty = 4.44$, whereas the Klein-Swift model uses $\eta = 0$ and $\varepsilon_\infty = 4.9$.

Liebe et al. [12] state that a second Debye relaxation frequency is needed to fit the experimental data for pure water above 100 GHz and they provide a double Debye fit in the frequency range up to 1 THz based on more recent measurements at high frequencies. At this point, it is not clear what the underlying physical process for such a second Debye relaxation is. It should be simply regarded as a necessary parameter, which is needed to provide an accurate fit for the dielectric constant over a wider frequency range than the single Debye model does while maintaining the necessary analyticity properties in the complex plane that are required by the dispersion relations. A similar approach had been undertaken in [3] who introduced the "spread factor" η, which has no relation to a real physical spread of the Debye relaxation frequency.

Stogryn et al. [13] provide a double Debye fit for both fresh and sea water in the salinity range between 0 and 38 ppt. They used their own laboratory measurement in the frequency range between 7 and 14 GHz, which they supplemented with existing measurements. Wang [8] found their model in good agreement with fresh water measurements from MIR at 89 and 220 GHz. Still, due to the lack of input data the validity of this model for sea water at higher frequencies needs a closer investigation. The first measurements of ε for sea water at frequencies above 30 GHz were done by Guillou et al. [7, 14], who found already above 80 GHz that it is insuffi-

cient to use a single Debye fit. None of these models have used data for supercooled pure water below $-4^{\circ}C$, so it is not clear if the models can be applied for supercooled clouds, whose temperatures can be as low as $-20^{\circ}C$ or even lower.

It is the purpose of this investigation:

1. To assess the performance of the various dielectric models for sea water by computing the emissivities and brightness temperatures of passive microwave ocean observations over a wide range of surface temperatures and comparing the results with the measurement. For this purpose, we have analyzed several months worth of SSM/I ocean brightness temperatures at 19.35, 37.0 and 85.5 GHz.
2. To provide a fit for the dielectric constant of sea water, which is compatible with both the SSM/I brightness temperature analysis and the validated models of Klein-Swift and Wentz at lower frequencies. The goal is to obtain a model, whose frequency range goes at least up to 100 GHz and, if possible, beyond. From what we mentioned earlier, such a model will necessarily need two Debye relaxation wavelengths.
3. To provide a smooth salinity interpolation between pure and sea water, whose salinity is typically around 35 ppt.
4. To extent the fit for pure to supercooled water with temperatures down to at least $-20^{\circ}C$, so that the model can be applied to compute the absorption of supercooled clouds.

Our paper is organized as follows:

In section 2 we present the SSM/I ocean brightness temperature analysis and statistical results of the comparison with the RTM calculations, which are done with various dielectric models. Section 3 describes the procedure and results for the double Debye fit of the pure water dielectric constant. We also discuss its implication for fresh water emissivities and liquid cloud water absorption and present a comparison with other dielectric models. In section 4 we describe the

procedure and results for the double Debye fit of the sea water dielectric constant, discuss its implication for ocean surface emissivities and compare with other models. Section 5 briefly summarizes our main results and conclusions.

II. SSM/I BRIGHTNESS TEMPERATURE ANALYSIS

A. Study Data Set

Our data set comprises ocean brightness temperatures that were measured by SSM/I F15 over the 4 months period June – September 2002. The data set also includes the measured Earth incidence angles (EIA). The Remote Sensing Systems (RSS) Version 5 algorithm [15] provides several ocean and atmospheric EDRs: Wind speed 10 m above the ocean surface W, columnar water vapor V and columnar liquid cloud water L. All of the EDRs have been carefully validated. The events are averaged into 0.25 deg latitude-longitude pixels and filtered for land, ice, and rain. Any pixel is discarded if there is land or ice in it or in any of the 8 surrounding pixels or if the SSM/I algorithm detects rain in it or in any of the 8 surrounding pixels. For a radiative transfer calculation, we need to know the vertical profiles of pressure, temperature, humidity and liquid cloud water density, which we obtain from the NCEP 6 hourly final analysis (FNL) at 1 deg resolution [16]. It contains 26 temperature and pressure and 21 humidity and cloud water density levels. We also obtain SST from the NCEP analysis. A tri-linear interpolation (latitude-longitude –time) is used to match the NCEP data with the SSM/I events. The values for the sea surface salinity S were obtained from [17] and we have used only pixels within the salinity range $20\ ppt \le S \le 40\ ppt$.

For studying the surface emissivity, it is desirable to deal with a planar (specular) surface, which is not roughened by wind. Though there exist numerous theoretical surface emission models for computing the emissivity of a wind roughened surface [18-21], these models are not

accurate enough for our purposes [11]. Fortunately, for SSM/I earth incidence angles and frequencies, the dependence of the vertical polarized emitted radiation is very small if the wind speed is not too large [22-25]. For winds below 5 m/s, the ocean surface for v-pol radiation can be regarded as specular. We therefore limit our study to v-pol radiation and events for which the SSM/I retrieved wind speed is less than 5 m/s.

We have performed our analysis using the water vapor absorption models of Rosenkranz 1998 [26]. Because the total vapor content in the NCEP analysis is known to be accurate to 10% at best, we are scaling the NCEP water vapor density profiles so that the total vertical integral equals the value V that is retrieved from SSM/I. For the brightness temperature analysis it is important to reduce possible cross talk errors between SST and V, which arises due to the global correlation between atmospheric moisture content and surface temperature. Areas with warm water likely produce moist atmospheres, whereas dry atmospheres most likely occur over cold water. When analyzing surface emissivity as function of SST, deficiencies in the vapor model could show up in a spurious deficiency of the surface emissivity model. Ideally, the crosstalk between SST and V is minimized, if V varies as little as possible within the analysis data set. As we shall see, the differences between the various dielectric models are most evident at cold temperatures, which warrants the use of dry atmospheric conditions for our analysis.

We have performed the analysis in 2 different vapor bins: $V < 10\ mm$ and $10\ mm < V < 20\ mm$. The validity of the Rosenkranz 1998 water vapor absorption model [26] under those dry conditions has been shown by various authors [26, 27]. The oxygen absorption model in our calculations is taken from Rosenkranz [28], which is based on the works of [29, 30].

The handling of the NCEP cloud water density profiles requires some special handling as well. The cloud water density recorded by NCEP refers to both liquid and ice clouds. Because at SSM/I frequencies the dielectric constant of ice is very small compared with the dielectric constant of liquid water, the SSM/I only measures absorption by liquid clouds. In order to extract

the liquid cloud density from the NCEP cloud water density profiles we assume that the cloud is water is completely in the liquid phase if the air temperature of the profile level is above $0^{\circ}C$ and completely in the ice phase if it is below $-20^{\circ}C$. For temperatures in between, we linearly interpolate the liquid density as a function of temperature. As it was the case for the total water vapor profiles, we do not use the absolute values of the NCEP liquid cloud water profiles but scale them so that the total vertical integral equals the value L that is retrieved from SSM/I. Furthermore, we limit L to 0.05 mm in order to avoid errors in the surface emissivity analysis due to uncertainties in the cloud water absorption. Globally, the probability density function for L has a strong peak at $L = 0$ and is rapidly decreasing for increasing L. This guarantees a sufficient number of events even if L is limited to these small values.

The model brightness temperature F is calculated from the radiative transfer equation:

$$F = T_{BU} + \tau E_0 T_S + \tau (1 - E_0) T_{BD} + \tau^2 (1 - E_0) T_C \qquad (4).$$

E_0 is the specular sea surface emissivity (1). $T_C = 2.7K$ is the cold space temperature. T_{BU} is the upwelling atmospheric brightness temperature and T_{BD} the downwelling atmospheric brightness temperature that is reflected at the sea surface. Both quantities are given as weighted integrals of the atmospheric temperature profiles $T(z)$ between the surface $z = 0$ and satellite altitude $z = H$:

$$\begin{aligned} T_{BU} &= \sec(\theta) \int_0^H dz \sum_I \alpha_I(z)\, T(z)\, \tau(z, H, \theta) \\ T_{BD} &= \sec(\theta) \int_0^H dz \sum_I \alpha_I(z)\, T(z)\, \tau(0, z, \theta) \end{aligned} \qquad (5),$$

where $\tau(h_1, h_2, \theta) \equiv \exp\left[-\sec(\theta) \int_{h_1}^{h_2} dz \sum_I \alpha_I(z) \right]$. The total atmospheric transmittance τ is given by $\tau = \tau(0, H, \theta)$. The α_I denote the atmospheric absorption coefficients for I = O (oxygen), V (water vapor) and L (liquid cloud water).

For our study, we have binned the results between $-2^{\circ}C$ and $+29^{\circ}C$ with respect to SST into 1 K temperature bins. For $V < 10\ mm$ the SST bin population peaks at $0^{\circ}C$ with almost 15,000 events and declines to about 150 at $25^{\circ}C$. For $10\ mm < V < 20\ mm$ the SST bin population increases from about 4,000 at $0^{\circ}C$ to about 19,000 at $17^{\circ}C$ and then decreases to about 100 at $28^{\circ}C$. Higher SST bins are not sufficiently populated.

B. Statistical Analysis of Measured versus Computed Brightness Temperatures

Figure 1 shows the difference between the SSM/I measured brightness temperatures T_B and the RTM calculation F as a function of the SST for the 4 SSM/I frequencies 19.35, 22.235 37.0 and 85.5 GHz. The RTM surface emissivities were calculated using the values for the sea water dielectric constant by Klein-Swift [1] (dash - 3 dots), Wentz [11] (long dashes), Stogryn et al. [13] (dash - dot) and Guillou et al. [7] (dot). In case of the Guillou model we have taken their single Debye fits at 19.35 and 37.0 GHz, whereas at 85.5 GHz we have used the linear temperature interpolation of their new measurements. As they have already pointed out, the single Debye fit is not applicable at 85.5 GHz. The figures in the upper panel were computed in the water vapor bin $V < 10\ mm$ and the ones in the lower panel in the water vapor bin $10\ mm < V < 20\ mm$. Ideally, the $T_B - F$ curve should be flat, i.e. independent on SST. A small finite constant bias is possible. It can arise from instrument calibration errors, for example in the spillover, or due to inaccuracies in the oxygen or water vapor absorption models. Table 1 contains several statistical parameters that are relevant for comparing T_B and F: The overall bias $\langle T_B - F \rangle$, the standard deviation $\sigma(T_B - F)$, the Pierson correlation coefficient r, slope m and y-axis intercept t of the linear regression $F = mT_B + t$. Figure 2 shows the histogram for $T_B - F$ using a bin size of 0.2 K and after subtracting the values of the overall biases. Ideally, the distribution is Gaussian with a narrow width, which only arises because of sensor noise.

The Wentz dielectric model performs best at 19.35 and 37.0 GHz. The 22.235 GHz channel is highly sensitive to water vapor and therefore the errors are dominated by errors in the water vapor retrievals. Nevertheless, we find a very good performance of the Wentz dielectric model, which is slightly better than the other models. The fact, that the results at 22.235 GHz are consistent with those at 19.35 GHz also indicate, that we are correctly modeling the effect of water vapor absorption on the observations. At 85.5 GHz, the measurements of Guillou et al. give the best result, which confirms our earlier analysis [25]. At 37 GHz, the Guillou model shows a relatively large negative bias, especially at cold SSTs, which is equivalent to overestimating the surface emissivity. On the other hand, at 85.5 GHz the Wentz model overestimates the emissivity in cold water. The Stogryn model slightly but still significantly overestimates the emissivity in cold water at both 37 and 85.5 GHz. The Klein-Swift model strongly overestimates the cold water emissivity at both 37 and 85.5 GHz.

The results of the SSM/I brightness temperature analysis provides us with a clear guideline for fitting the dielectric constant of sea water with 35 ppt salinity using two Debye relaxation frequencies: Below 37 GHz we want to be consistent with the Wentz [11] model and at 85.5 GHz with the results of Guillou et al. [7].

III. THE DIELECTRIC CONSTANT OF PURE WATER

A. Two Debye Relaxation Fit for Pure Water

As stated above, we fit the dielectric constant with a double Debye relaxation law. The general form reads:

$$\varepsilon(T,S) = \frac{\varepsilon_S(T,S) - \varepsilon_1(T,S)}{1 + i\,\nu/\nu_1(T,S)} + \frac{\varepsilon_1(T,S) - \varepsilon_\infty(T,S)}{1 + i\,\nu/\nu_2(T,S)} + \varepsilon_\infty(T,S) - i\frac{\sigma(T,S)}{(2\pi\varepsilon_0)\nu} \quad (6).$$

We have chosen the convention in which the imaginary part of ε is negative. The symbols and

units are as follows: $i=\sqrt{-1}$, ν is the radiation frequency [in GHz], $\varepsilon_S(T,S)$ the static (zero frequency) dielectric constant, $\varepsilon_1(T,S)$ the intermediate frequency dielectric constant and $\varepsilon_\infty(T,S)$ is dielectric constant at infinite frequencies. $\nu_1(T,S)$ and $\nu_2(T,S)$ are first and second Debye relaxation wavelengths [in GHz], respectively. $\sigma(T,S)$ is the conductivity of water [in S/m] and $\frac{1}{2\pi\varepsilon_0}=17.97510\frac{GHz\ m}{S}$. The temperature T is in $^\circ C$ and the salinity S in ppt.

In this section we will consider pure water where $S=0$ and $\sigma(T,S=0)=0$.

The static dielectric constant for pure water $\varepsilon_S(T,S=0)$ has been measured by several groups over the temperature range between $-21^\circ C$ and $+40^\circ C$ [31-35]. Their results agree within 0.2%. For reference, we use the fit given in [13]:

$$\varepsilon_S(T,S)=\frac{3.70886\cdot 10^4-8.2168\cdot 10^1 T}{4.21854\cdot 10^2+T} \qquad (7).$$

This fit differs by the one of [11] by 0.02% or less between $0^\circ C$ and $+40^\circ C$. At $-40^\circ C$, which is outside the measurement range, the difference is 0.13%.

For the temperature dependence of the 4 fit parameters ε_1, ε_∞, ν_1 and ν_2 we make the ansatz:

$$\begin{aligned}
\varepsilon_1(T,S=0)&=a_0+a_1T+a_2T^2\\
\nu_1(T,S=0)&=\frac{45+T}{a_3+a_4T+a_5T^2}\\
\varepsilon_\infty(T,S=0)&=a_6+a_7T\\
\nu_2(T,S=0)&=\frac{45+T}{a_8+a_8T+a_{10}T^2}
\end{aligned} \qquad (8).$$

The form for the two relaxation frequencies ν_1 and ν_2 is inspired by the discussion in [36], which suggests that supercooled water undergoes a phase transition at a critical temperature $T_{crit}=-45^\circ C$. This would lead to a singularity in the Debye relaxation time τ, which is the in-

verse of the relaxation frequency: $\tau_R = {}^{1}\!/_{\nu_R} \sim \left(T/T_{crit} - 1\right)^{-\alpha}$. The value of the critical exponent α in [36] lies between 1 and 2.

The data we are using for our fit are listed in the Appendix (Table 2). Following, [12] we have produced metadata from the single Debye fit of Kaatze and Uhlendorf [37] for frequencies between 5 and 60 GHz. Other than in [12], we have not used metadata for higher frequencies from this source, because [37] have reported only one measurement above 60 GHz and we anticipate that the single Debye fit is getting inaccurate at higher frequencies. As [12] and [13] did, we rely on the measurements of Hasted et al. [38] for frequencies between 100 and 500 GHz but we did not go beyond 500 GHz. Below 100 GHz we have included the measurements by Barthel et al. at $25^{\circ}C$ [39]. The only measurements for supercooled water were done by Bertolini et al. at 9.61 GHz and comprise the temperature range between $-21^{\circ}C$ and $+31^{\circ}C$ [40]. We did include this data set in our fit, which was not done neither in [12] nor [13].

The 11 fit parameters $a_i, i = 0,\ldots,10$ are determined by minimizing the square deviation between data and fit function (6)-(8) for real and imaginary parts of the dielectric constant:

$$Q^2 = \sum_i w_i^1 \left[\mathrm{Re}\left(\varepsilon_i^{meas} - \varepsilon_i^{fit}\right)\right]^2 + w_i^2 \left[\mathrm{Im}\left(\varepsilon_i^{meas} - \varepsilon_i^{fit}\right)\right]^2 \qquad (9).$$

The index i runs over all data that are listed in Table 2. We have used equal weights $w_i^1 = w_i^2 = 1$.

After numerical minimization of (9) we obtain the values for $a_i, i = 0,\ldots,10$ in Table 3. Table 4 lists the $\sqrt{Q^2}$ values between the experimental data sets from Table 2 and various models including our new fit. Figure 3 shows real and imaginary part of ε at a temperature of $0^{\circ}C$ as function of frequency for our new fit and the models mentioned above. Figure 4, Figure 5, Figure 6 and Figure 7 display the temperature dependence of the parameters ν_1, ν_2, ε_1 and ε_∞.

We want to stress that the lack of measurements for supercooled water at high frequencies

does not allow a safe determination of the second Debye relaxation frequency ν_2 and the parameter ε_∞ at those temperatures. Our values as well as the value for the dielectric constant at larger frequencies can therefore be merely regarded as an extrapolation from temperatures above $0^\circ C$. This will necessarily limit the predictive power of our and any other model in these cases.

B. Implications for the Specular Emissivity of Fresh Water

In order to quantitatively assess the differences in the prediction of fresh water surface emissivities between the various models, we have plotted the surface emitted brightness temperatures $E_0\left(T = T_S, S = 0\right) \cdot T_S$ as a function of T_S at 37, 85.5 and 170 GHz and v-pol and h-pol at 53 deg EIA as well as for nadir observations in Figure 8. The plot shows the differences between Wentz [11] (dashed), Stogryn [13] (dashed-dot), Klein-Swift [1] (dashed-dot-dot) and Liebe [12] (dotted) and the result of our new fit. At 37 GHz our new result is within 1 K of both the Liebe and the Stogryn models. At 85.5 GHz we are in very good agreement with Liebe at all temperatures and at high temperatures also with Stogryn. At cold temperatures the Stogryn emissivity is about 2 K smaller than ours. The differences between our new fit and the models of Liebe and Stogryn in cold water increase to about 3 K at 170 GHz. We have checked that at higher frequencies the discrepancies between the Stogryn model and our new fit are decreasing. Above 260 GHz the emitted brightness temperatures of our fit are within 1 K of the Stogryn model over the whole temperature range. It is also obvious, that the single Debye models (Klein-Swift and Wentz) predict both much larger emissivities over cold water at 170 GHz than Liebe, Stogryn or our new fit.

The estimates of Wang [8] for emissivities of cold, fresh water, which are based on near nadir MIR airborne measurements over the Great Lakes at 89 and 220 GHz seem to slightly favor the Stogryn model over Liebe's. At 150 GHz all of the model emissivity predictions are by at least

3 K larger than Wang's data if he is using the Rosenkranz 1998 water vapor absorption for retrieving. Wang also states that the ε value of Guillou et al. [7] at 89 GHz and low temperatures is inconsistent with his measurements. This differs from our observation in section II, which found that Guillou's value provided the best fit for the SSM/I ocean brightness temperatures at 85.5 GHz. It should be noted that Wang's data are all taken over cold water whose temperature is close to freezing and it is therefore difficult to analyze the temperature behavior of the emissivity model as we did in Figure 1. Clearly, more measurements of the fresh water emissivity at high frequency would be needed to resolve these inconsistencies and validate one of the models.

C. Implications for Liquid Cloud Water Absorption

In order to assess the implications of our new fit for the liquid cloud water absorption we have repeated the SSM/I brightness temperature analysis for cold clouds and included columnar cloud water contents up to 0.18 mm. We have limited the columnar water vapor to below 40 mm in order to avoid possible uncertainties, which could arise from deficiencies in the vapor absorption model or errors in the vapor retrievals. We have binned the difference between measured and RTM brightness temperatures $T_B - F$ with respect to the total cloud water L as well as the average temperature T_{cloud} of the liquid cloud, which we have obtained from the NCEP profiles. The population in the temperature bins ranges from 2,000 at $T_{cloud} = -15^{\circ}C$ to over 90,000 at $T_{cloud} = +6^{\circ}C$. The population in the cloud water bins ranges from 2,000 at $L = 0.18\ mm$ to over 280,000 at $L = 0.02\ mm$. Figure 9 shows the results at 85.5 GHz. Because we want to test the influence of ε on the cloud water absorption and not the surface emissivity we have used the emissivity model of Guillou et al. [7] for all four curves. We had shown in section II.B that this model provides the best results for the ocean surface emissivity at 85.5 GHz.

It is obvious that the liquid cloud water absorption (2) is less sensitive to the value of the dielectric constant than the surface emissivity (1). Our new fit gives an absorption very close to the one predicted by Liebe's model. The plot also suggests that the cloud water absorption obtained by the dielectric model of Stogryn et al. is getting too small as the cloud water temperature decreases. The absorption using the Wentz model is slightly larger than with our new model but the overall temperature dependence is almost the same. We have also checked that at 37 GHz the four curves differ by less than 0.35 K over the whole range of T_{cloud}. Though neither Liebe et al. nor Wentz had included data for supercooled water in their fits for ε, we can conclude that their dielectric models perform nevertheless very well for frequencies below 100 GHz and average cloud temperatures above $-20^{\circ}C$. The discrepancies between the models for cloud water absorption can get very large at lower temperatures due to the very different analytic forms of the model constants and the fact that no laboratory data exist for those low temperatures [41]. The differences between the various model predictions for supercooled cloud water absorption also increases with increasing frequency [41]. In the absence of any reliable cloud water absorption measurements in these cases it is currently not possible to perform a better validation. It should also be noted the cloud water absorption that at 37 and 85.5 GHz is mainly sensitive to the real part of the dielectric constant and almost insensitive to its imaginary part. For $T_{cloud} = -10^{\circ}C$ an increase of $\mathrm{Re}(\varepsilon)$ by 10% decreases the total cloud water absorption by about 8%, whereas an increase of $\mathrm{Im}(\varepsilon)$ by 10% increases the total cloud absorption by only 0.7%. As we will discuss in further detail in the next section, the surface emissivity is mainly sensitive to $\mathrm{Im}(\varepsilon)$, especially at higher frequencies. This means that surface emissivity and cloud water absorption probe in fact different parts of the dielectric constant.

IV. THE DIELECTRIC CONSTANT OF SEA WATER

As a final step we now proceed to the fit for the dielectric constant of sea water based on the ocean surface emissivity analysis from section II. The double Debye relaxation law (6) requires to determine the temperature and salinity dependence of the 6 parameters $\varepsilon_S(T,S)$, $\varepsilon_1(T,S)$, $\varepsilon_\infty(T,S)$, $\nu_1(T,S)$, $\nu_2(T,S)$ and $\sigma(T,S)$ with the constraints (7) and (8) at $S=0$.

A. The Conductivity of Sea Water

The conductivity of sea water $\sigma(T,S)$ has been measured in laboratory experiments. We use the most updated regression given in [13], which we repeat for reference here. In the relevant salinity range $20\,ppt \le S \le 40\,ppt$ it differs by less than 0.5% from the expression given by Wentz [11].

$$\sigma(T,S) = \sigma(T,S=35)\cdot R_{15}(S)\cdot\frac{R_T(S)}{R_{15}(S)} \qquad (10)$$

where:

$$\sigma(T,S=35) = 2.903602 + 8.607\cdot10^{-2}\cdot T + 4.738817\cdot10^{-4}\cdot T^2 - 2.991\cdot10^{-6}\cdot T^3 + 4.3047\cdot10^{-9}\cdot T^4 \qquad (11)$$

$$R_{15}(S) = S\cdot\frac{(37.5109 + 5.45216\cdot S + 1.4409\cdot10^{-2}\cdot S^2)}{(1004.75 + 182.283\cdot S + S^2)} \qquad (12)$$

$$\frac{R_T(S)}{R_{15}(S)} = 1 + \frac{\alpha_0(T-15)}{(\alpha_1 + T)} \qquad (13)$$

$$\alpha_0 = \frac{\left(6.9431 + 3.2841\cdot S - 9.9486\cdot10^{-2}\cdot S^2\right)}{\left(84.850 + 69.024\cdot S + S^2\right)} \qquad (14)$$

$$\alpha_1 = 49.843 - 0.2276\cdot S + 0.198\cdot10^{-2}\cdot S^2 \qquad (15).$$

B. Fit Ansatz

For the remaining five constants we make the ansatz:

$$\begin{aligned}
\varepsilon_S(T,S) &= \varepsilon_S(T,S=0)\cdot\exp\left[b_0 S + b_1 S^2 + b_2 TS\right] \\
\nu_1(T,S) &= \nu_1(T,S=0)\cdot\left[1 + S\cdot\left(b_3 + b_4 T + b_5 T^2\right)\right] \\
\varepsilon_1(T,S) &= \varepsilon_1(T,S=0)\cdot\exp\left[b_6 S + b_7 S^2 + b_8 TS\right] \qquad (16). \\
\nu_2(T,S) &= \nu_2(T,S=0)\cdot\left[1 + S\cdot\left(b_9 + b_{10} T\right)\right] \\
\varepsilon_\infty(T,S) &= \varepsilon_\infty(T,S=0)\cdot\left[1 + S\cdot\left(b_{11} + b_{12} T\right)\right]
\end{aligned}$$

Other than in earlier models, we have also allowed a salinity dependence for ε_∞.

The 13 fit parameters $b_i, i = 0,\ldots,12$ are again determined by minimizing the square deviation (9) between data and fit function (6)-(8) for real and imaginary parts of the dielectric constant.

C. Metadata and Weights

For performing the minimization we create a metadata set, which will allow us to obtain a value for the surface emissivity from our fit that is consistent with results of the SSM/I brightness temperature analysis in section II: For frequencies up to 37 GHz we want to be as close as possible to the model of Wentz [11] and at 85.5 GHz to the value of Guillou et al. [7].

It is important to note that the sensitivity of the specular emissivity E_0 to $\mathrm{Im}(\varepsilon)$ is much stronger than to $\mathrm{Re}(\varepsilon)$ and this discrepancy increases with increasing frequency (c.f. Table 5). Form this it follows that at higher frequencies (37 GHz and especially 85.5 GHz) the result in section II allows us mainly to pin down $\mathrm{Im}(\varepsilon)$, whereas larger deviations of $\mathrm{Re}(\varepsilon)$ between the final fit and metadata are allowed without changing the value of the surface emissivity. This fact provides us with an important guideline for choosing appropriate weights w_i^1 and w_i^2 in (9). The final choice of the metadata set and the weights is done by trial and error so that the final result matches our objective best. The choice of the metadata and their weights are as follows:

1. The frequencies of the metadata points are taken at 3.0, 7.0, 10.0, 18.0, 24.0, 37.0, 85.5 and 89.0 GHz.
2. For each frequency we chose the following values for surface temperature: $-2^{\circ}C$, $+12^{\circ}C$, $+20^{\circ}C$ and $+30^{\circ}C$.
3. For 37 GHz and below we chose the following values for salinity: 10, 20, 30, 35 and 40 ppt. The values of ε are computed using the Wentz [11] model.
4. At 85.5 and 89.0 GHz we have set the salinity to 35 ppt and taken the values of ε given by Guillou et al. [7]. These data do not allow a study of the salinity dependence of ε. As a consequence, in our ansatz (16), we have fitted the constants ν_2 and ε_∞, which govern the high frequency behaviour of ε, only with a linear salinity dependence.
5. For each value of frequency and temperature we have supplemented the data set with an ε for pure water ($S = 0$) using our new fit from section III.
6. We are suing the weights: $w_i^1 = w_i^2 = 1$ for $\nu \le 24\ GHz$, $w_i^1 = 1$ and $w_i^2 = 5$ for $\nu = 37\ GHz$, and $w_i^1 = 0$ and $w_i^2 = 10$ for $\nu \ge 85.5\ GHz$.

The choices 3 and 5 imply that we have not used the values for $\mathrm{Re}(\varepsilon)$ from [7], but strongly weighted their values for $\mathrm{Im}(\varepsilon)$ instead. The reason for this choice is the fact that $E_0 T_S$ is much less sensitive to $\mathrm{Re}(\varepsilon)$ than to $\mathrm{Im}(\varepsilon)$, as mentioned earlier. Moreover, the values for $\mathrm{Re}(\varepsilon)$ at 85.5 GHz and 89.0 GHz given in [7] differ by 10%, which is obviously too large. This points to some potential uncertainty in their measurement of $\mathrm{Re}(\varepsilon)$. We have therefore decided to choose the weights at 85.5 GHz and 89.0 GHz in a way to ensure an optimal fit for $E_0 T_S$ rather than for $\mathrm{Re}(\varepsilon)$.

D. Results

Minimizing the value of Q^2 between this metadata set and the fit function leads to the values for the fit parameters $b_i, i = 0,\ldots,12$ listed in Table 6. Figure 10 shows the final result for $\mathrm{Re}(\varepsilon)$ and $\mathrm{Im}(\varepsilon)$ as a function of frequency at $T_S = 0^\circ C$ and $S = 35\ ppt$ that we obtain from our fit and compares with the results of the other models. The temperature dependences of the static dielectric constant ε_S and the first Debye relaxation frequency ν_1 at $S = 35\ ppt$ are displayed in Figure 11 and Figure 12, respectively. The short segments in Figure 5, Figure 6 and Figure 7, respectively, show the temperature dependence of the parameters ν_2, ε_1 and ε_∞ at $S = 35\ ppt$.

E. Implications for the Specular Emissivity of Sea Water

Most important for our purposes are the implications of our new fit for the ocean surface emissivities. From the values in Table 1 and the curves in Figure 1 and Figure 2 it is obvious that for the SSM/I v-pol brightness temperatures our new fit is matching the results of Wentz below 37 GHz and the results of Guillou et al. at 85.5 GHz very accurately. Figure 13 shows the difference for $E_0(T_S, S = 35) \cdot T_S$ between the different models and our new fit as a function of T_S at 37, 85.5 and 170 GHz for v-pol and h-pol at 53 deg EIA as well as for nadir observations. We see that the agreement with the Wentz model at low frequencies and the Guillou value at 85.5 GHz also holds for h-pol and nadir observations. At 170 GHz our new model agrees well with the prediction of Stogryn. Currently, there are neither laboratory measurements nor microwave sensor observations for the dielectric constant of sea water available at frequencies above 100 GHz.

V. SUMMARY AND CONCLUSIONS

The main issue of this study was to provide an updated fit for the dielectric constant of pure and sea water that can be used in the theory of radiative transfer of ocean emitted microwave radiation and is valid within a larger frequency and temperature range than the model of Klein-Swift, which has been mainly used so far. Our new fit uses two Debye relaxation frequencies: the lower one at around 20 GHz and the upper one at around 200 GHz. For sea water our new model is consistent with the model of Wentz [11] below 37 GHz and with the measurements of $\mathrm{Im}(\varepsilon)$ by Guillou et al. [7] at 85.5 GHz and 89 GHz. For pure water we have used a large data set of laboratory measurements in the frequency range up to 500 GHz and in the temperature range between $-20^{\circ}C$ and $+40^{\circ}C$, which includes supercooled water. Our fit smoothly interpolates the dielectric constant as a function of salinity between 0 and 40 ppt.

We have validated our new model using the SSM/I brightness temperature analysis. We have shown that below 100 GHz our dielectric model gives very accurate values for the ocean surface emissivities between $-2^{\circ}C$ and $+29^{\circ}C$ as well as the liquid cloud water absorption above $-15^{\circ}C$. Due to the lack of measurements, uncertainties still remain in some cases.

ACKNOWLEDGEMENT

This work has been funded by the Boeing/AER investigation for CMIS (Integrated Program Office contract # F04701-02-C-0502). We are thankful to Phil Rosenkranz (MIT) for the FORTRAN codes for calculating the water vapor [26] and oxygen absorption coefficients and to J. Wang (NASA Goddard) for the FORTRAN code of the dielectric model [13].

APPENDIX

Table 2 lists the experimental data that we used for fitting the double Debye relaxation model of pure water.

FIGURES

Figure 1: SSM/I measured minus computed ocean brightness temperatures as a function of surface temperature using various dielectric models at 19.35, 37.0 and 85.5 GHz and vertical polarization. The bin size is 1 Kelvin. The upper panel was computed using the water vapor bin $V < 10\ mm$ and the lower panel using the water vapor bin $10\ mm < V < 20\ mm$.

Figure 2: Histogram of SSM/I measured minus computed ocean brightness temperatures as a function of surface temperature using various dielectric models at 19.35, 37.0 and 85.5 GHz and vertical polarization. The bin size is 0.2 Kelvin. The upper panel was computed for the water vapor bin $V < 10\ mm$ and the lower panel for the water vapor bin $10\ mm < V < 20\ mm$.

Figure 3: Real and Imaginary part of the dielectric constant for pure water with a temperature of $0^{\circ}C$ as function of frequency for various dielectric models.

Figure 4: The first Debye relaxation frequency ν_1 of pure water as function of surface temperature for various dielectric models.

Figure 5: The second Debye relaxation frequency ν_2 as function of surface temperature for various dielectric models. The long segments correspond to pure water and the short segments to seawater with a salinity of 35 ppt. The model of [13] has no salinity dependence and the model of [12] is for pure water only.

Figure 6: The parameter ε_1 as function of surface temperature for various dielectric models. The long segments correspond to pure water and the short segments to seawater with a salinity of 35 ppt.

Figure 7: The parameter ε_∞ as function of surface temperature for various dielectric models. The long segments correspond to pure water and the short segments to seawater with a salinity of 35 ppt. The model of [13] has no salinity dependence and the model of [12] is for pure water only.

Figure 8: Surface emitted brightness temperature, defined as product of surface emissivity and surface temperature [in Kelvin] for pure water. The plot shows the differences between various models and our new result as a function of surface temperature: Wentz [11] (dashed), Stogryn [13] (dashed-dot), Klein-Swift [1] (dashed-dot-dot) and Liebe [12] (dotted).

Figure 9: SSM/I measured minus computed 85.5 GHz v-pol ocean brightness temperatures as a function of columnar liquid cloud water [bin size 0.01 mm] and average cloud temperature [bin size 1 Kelvin] for cold clouds using various models for the cloud water dielectric constant.

Figure 10: Real and Imaginary part of the dielectric constant for sea water with a salinity of 35 ppt and a temperature of $0^\circ C$ as function of frequency for various dielectric models. The star symbol corresponds to the measured values in [7] and the dotted line to their single Debye fit at low frequencies.

Figure 11: The static dielectric constant ε_S of sea water with a salinity of 35 ppt as function of surface temperature for various dielectric models.

Figure 12: The first Debye relaxation frequency ν_1 of sea water with a salinity of 35 ppt as function of surface temperature for various dielectric models.

Figure 13: Surface emitted brightness temperature, defined as product of surface emissivity and surface temperature [in Kelvin] for sea water (S= 35 ppt). The plot shows the differences

between various models and our new result as a function of surface temperature: Wentz [11] (dashed), Stogryn [13] (dashed-dot), Klein-Swift [1] (dashed-dot-dot) and Guillou [7] (dotted: using their single Debye fit at 37 GHz and the measured value at 85.5 GHz).

TABLES

		V < 10mm					10 mm < V < 20 mm				
FREQ	MODEL	BIAS	SDEV	r	m	t	BIAS	SDEV	r	m	t
19.35	NEW FIT	1.383	0.659	0.916	0.842	26.872	1.400	0.800	0.967	0.898	17.601
	Wentz [10, 11]	1.453	0.656	0.917	0.852	24.970	1.410	0.791	0.967	0.908	15.640
	Guillou fit [7]	-0.583	0.805	0.871	0.739	47.249	-0.125	0.875	0.960	0.876	23.117
	Stogryn [13]	0.543	0.694	0.906	0.818	32.043	0.678	0.808	0.966	0.894	19.034
	Klein-Swift [1]	0.780	0.813	0.869	0.728	47.996	1.343	0.926	0.957	0.837	28.854
22.235	NEW FIT	0.286	0.761	0.977	0.988	1.977	0.040	1.160	0.976	0.986	2.930
	Wentz [10, 11]	0.389	0.764	0.977	0.992	1.158	0.083	1.161	0.976	0.990	1.907
	Guillou fit [7]	-1.710	0.838	0.972	0.917	17.462	-1.321	1.199	0.974	0.964	8.732
	Stogryn [13]	-0.522	0.779	0.976	0.964	7.365	-0.572	1.161	0.976	0.978	5.046
	Klein-Swift [1]	-0.411	0.810	0.974	0.929	13.935	-0.091	1.196	0.974	0.958	8.770
37.0	NEW FIT	-1.231	0.515	0.918	0.927	16.145	-1.209	0.795	0.894	0.893	23.334
	Wentz [10, 11]	-1.188	0.572	0.903	0.947	11.989	-1.042	0.818	0.888	0.891	23.475
	Guillou fit [7]	-4.282	0.991	0.786	0.995	5.384	-3.539	1.028	0.834	0.881	28.041
	Stogryn [13]	-2.328	0.690	0.870	0.959	10.581	-2.105	0.838	0.882	0.882	26.339
	Klein-Swift [1]	-2.731	0.922	0.808	1.000	2.738	-1.859	1.129	0.789	0.802	42.585
85.5	NEW FIT	-1.414	1.163	0.918	0.784	52.666	-1.121	1.686	0.909	0.854	37.025
	Wentz [10, 11]	-2.828	1.491	0.867	0.638	88.872	-1.528	1.879	0.885	0.764	59.818
	Guillou (meas.) [7]	-1.488	1.136	0.921	0.801	48.886	-1.339	1.649	0.914	0.876	31.864
	Stogryn [13]	-2.600	1.259	0.907	0.723	68.468	-1.937	1.695	0.908	0.828	44.436
	Klein-Swift [1]	-4.645	1.634	0.841	0.572	106.366	-2.772	1.982	0.873	0.710	74.358

Table 1: Statistical results for the v-pol model function F computed with various dielectric models versus SSM/I measured brightness temperature T_B: Bias of $T_B - F$, standard deviation of $T_B - F$, linear correlation coefficient r, slope m and y-axis interception t [in Kelvin] of the linear regression $F = mT_B + t$. The fit was performed in 2 different water vapor bins: $V < 10\,mm$ and $10\,mm < V < 20\,mm$. The values of Guillou [7] refer to their single Debye fit at 19.35, 22.235 and 37 GHz and to their new measurement at 85.5 GHz.

Source	$\nu\,[GHz]$	$T_S\,[^\circ C]$	$\mathrm{Re}(\varepsilon)$ measured	$\mathrm{Re}(\varepsilon)$ fit	$\mathrm{Im}(\varepsilon)$ measured	$\mathrm{Im}(\varepsilon)$ fit
Barthel et al. [39]	1.7	25	76.92	77.83	6.64	6.42
Barthel et al. [39]	2.05	25	76.44	77.58	7.92	7.71
Barthel et al. [39]	2.5	25	76.66	77.18	9.40	9.36
Barthel et al. [39]	4	25	74.92	75.35	14.44	14.59
Barthel et al. [39]	4.45	25	74.49	74.66	15.55	16.07
Barthel et al. [39]	4.6	25	73.77	74.42	17.17	16.55
Barthel et al. [39]	5.35	25	73.23	73.12	18.41	18.89
Barthel et al. [39]	5.8	25	72.58	72.27	19.65	20.22
Barthel et al. [39]	8.5	25	65.96	66.4	26.82	27.02
Barthel et al. [39]	9.2	25	64.89	64.73	28.35	28.44
Barthel et al. [39]	10	25	63.01	62.78	29.81	29.89
Barthel et al. [39]	11.2	25	59.98	59.83	31.58	31.74
Barthel et al. [39]	12	25	57.95	57.86	32.72	32.77
Barthel et al. [39]	13	25	55.47	55.42	33.60	33.84
Barthel et al. [39]	14	25	53.03	53.03	34.37	34.70
Barthel et al. [39]	15	25	50.83	50.71	35.11	35.35
Barthel et al. [39]	16.5	25	47.54	47.38	35.81	36.01
Barthel et al. [39]	17.5	25	45.27	45.27	35.76	36.27
Barthel et al. [39]	27	25	29.37	30.01	33.89	34.40
Barthel et al. [39]	30	25	26.12	26.74	32.55	33.08
Barthel et al. [39]	33	25	23.56	24.01	31.22	31.68
Barthel et al. [39]	36	25	21.65	21.73	29.96	30.29
Barthel et al. [39]	39	25	19.53	19.83	28.57	28.92
Barthel et al. [39]	60	25	12.87	12.4	21.38	21.36
Barthel et al. [39]	66	25	11.81	11.32	19.90	19.80
Barthel et al. [39]	72	25	11.17	10.46	18.19	18.43
Barthel et al. [39]	79	25	10.04	9.67	17.68	17.06
Barthel et al. [39]	89	25	8.35	8.81	15.45	15.42
Kaatze et al. [37]	5	-4	63.81	64.56	38.38	38.41
Kaatze et al. [37]	10	-4	36.13	36.75	40.07	40.61
Kaatze et al. [37]	10	0	42.51	42.12	40.89	40.89
Kaatze et al. [37]	10	10	53.40	53.46	38.22	38.17
Kaatze et al. [37]	10	20	61.04	60.68	32.59	32.79
Kaatze et al. [37]	10	30	64.18	64.07	27.12	27.12
Kaatze et al. [37]	20	0	19.55	19.34	30.79	30.69
Kaatze et al. [37]	20	10	27.61	27.77	35.25	35.21
Kaatze et al. [37]	20	20	36.91	36.51	36.81	36.72
Kaatze et al. [37]	20	30	43.92	43.83	35.70	35.47
Kaatze et al. [37]	30	0	12.48	12.37	22.65	22.63
Kaatze et al. [37]	30	10	17.17	17.39	27.86	27.90
Kaatze et al. [37]	30	20	23.76	23.52	32.00	31.84
Kaatze et al. [37]	30	30	29.76	29.86	34.12	33.78
Kaatze et al. [37]	40	0	9.65	9.58	17.62	17.70
Kaatze et al. [37]	40	10	12.54	12.78	22.35	22.46
Kaatze et al. [37]	40	20	17.04	16.93	26.85	26.74

Kaatze et al. [37]	40	30	21.38	21.65	30.17	29.86
Kaatze et al. [37]	50	10	10.17	10.41	18.47	18.67
Kaatze et al. [37]	50	20	13.35	13.32	22.74	22.71
Kaatze et al. [37]	50	30	16.40	16.78	26.31	26.08
Kaatze et al. [37]	60	10	8.81	9.05	15.68	15.94
Kaatze et al. [37]	60	20	11.17	11.16	19.57	19.63
Kaatze et al. [37]	60	30	13.29	13.74	23.06	22.92
Bertolini et al. [40]	9.61	-21	15.40	15.56	29.00	29.61
Bertolini et al. [40]	9.61	-20	17.00	16.97	30.80	31.01
Bertolini et al. [40]	9.61	-19	17.60	17.42	31.50	31.43
Bertolini et al. [40]	9.61	-18	19.20	19.04	32.50	32.84
Bertolini et al. [40]	9.61	-18	19.50	19.28	32.40	33.03
Bertolini et al. [40]	9.61	-16	21.70	21.37	34.70	34.61
Bertolini et al. [40]	9.61	-11	27.70	27.62	39.10	38.16
Bertolini et al. [40]	9.61	-8	31.80	31.55	40.80	39.63
Bertolini et al. [40]	9.61	-6	35.60	35.38	41.60	40.58
Bertolini et al. [40]	9.61	-3	39.80	39.71	42.20	41.10
Bertolini et al. [40]	9.61	0	43.10	43.61	41.80	41.05
Bertolini et al. [40]	9.61	1	45.70	46.03	41.00	40.77
Bertolini et al. [40]	9.61	3	48.40	48.1	40.70	40.38
Bertolini et al. [40]	9.61	6	51.70	51.79	38.70	39.25
Bertolini et al. [40]	9.61	10	55.20	55.19	37.90	37.66
Bertolini et al. [40]	9.61	14	57.90	58.27	35.90	35.62
Bertolini et al. [40]	9.61	17	60.30	60.54	33.10	33.59
Bertolini et al. [40]	9.61	32	65.80	65.17	25.00	25.22
Hasted et al. [38]	176	10	5.71	5.79	7.10	6.36
Hasted et al. [38]	176	20	5.73	5.98	7.79	7.81
Hasted et al. [38]	176	30	6.28	6.21	8.99	9.19
Hasted et al. [38]	176	40	6.24	6.57	9.98	10.35
Hasted et al. [38]	205	10	5.41	5.57	6.24	5.64
Hasted et al. [38]	205	20	5.58	5.69	7.11	6.86
Hasted et al. [38]	205	30	5.85	5.84	8.16	8.01
Hasted et al. [38]	205	40	5.78	6.13	9.00	8.97
Hasted et al. [38]	234	10	5.35	5.39	5.57	5.10
Hasted et al. [38]	234	20	5.55	5.46	6.37	6.14
Hasted et al. [38]	234	30	5.60	5.58	7.34	7.10
Hasted et al. [38]	234	40	5.68	5.83	8.16	7.92
Hasted et al. [38]	264	10	5.29	5.23	4.95	4.66
Hasted et al. [38]	264	20	5.35	5.28	5.61	5.54
Hasted et al. [38]	264	30	5.36	5.38	6.43	6.35
Hasted et al. [38]	264	40	5.51	5.61	7.19	7.05
Hasted et al. [38]	293	10	5.21	5.1	4.44	4.31
Hasted et al. [38]	293	20	5.16	5.14	4.94	5.07
Hasted et al. [38]	293	30	5.21	5.23	5.54	5.77
Hasted et al. [38]	293	40	5.34	5.46	6.32	6.38
Hasted et al. [38]	322	10	5.15	4.98	4.14	4.01
Hasted et al. [38]	322	20	5.10	5.02	4.50	4.67

Hasted et al. [38]	322	30	5.16	5.12	5.05	5.28
Hasted et al. [38]	322	40	5.30	5.35	5.76	5.82
Hasted et al. [38]	351	10	5.05	4.88	3.78	3.76
Hasted et al. [38]	351	20	5.04	4.92	4.20	4.34
Hasted et al. [38]	351	30	5.12	5.03	4.72	4.87
Hasted et al. [38]	351	40	5.26	5.26	5.32	5.35
Hasted et al. [38]	381	10	5.02	4.78	3.46	3.52
Hasted et al. [38]	381	20	4.94	4.84	3.85	4.03
Hasted et al. [38]	381	30	5.13	4.96	4.28	4.50
Hasted et al. [38]	381	40	5.16	5.19	4.88	4.94
Hasted et al. [38]	410	10	4.86	4.7	3.57	3.33
Hasted et al. [38]	410	20	5.02	4.77	3.56	3.78
Hasted et al. [38]	410	30	5.25	4.9	3.97	4.20
Hasted et al. [38]	410	40	5.04	5.13	4.54	4.60

Table 2: Experimental data for the dielectric constant of pure water, which we have used in the fit. For comparison, the values obtained with our new fit are also displayed.

i	a_i
0	5.7230 E00
1	2.2379 E-02
2	-7.1237 E-04
3	5.0478 E00
4	-7.0315 E-02
5	6.0059 E-04
6	3.6143 E00
7	2.8841 E-02
8	1.3652 E-01
9	1.4825 E-03
10	2.4166 E-04

Table 3: Parameters of the fit (8) for pure water.

	Liebe et al. [12]	Stogryn et al. [13]	Wentz [10, 11]	Klein-Swift [1]	NEW FIT
Barthel et al. [39]	0.63	0.56	0.70	0.76	0.57
Kaatze et al. [37]	0.29	0.57	0.63	0.58	0.36
Bertolini et al. [40]	1.59	3.22	2.44	1.59	0.68
Hasted et al. [38]	0.32	0.31	0.72	0.71	0.29

Table 4: $\sqrt{Q^2}$ between experimental data sets and various fits for the dielectric constant of pure water.

$v\,[GHz]$	$\left.\frac{\Delta(E_0 T_S)}{\Delta \mathrm{Re}(\varepsilon)}\right\|_{T_s=273.15K}\,[K]$	$\left.\frac{\Delta(E_0 T_S)}{\Delta \mathrm{Im}(\varepsilon)}\right\|_{T_s=273.15K}\,[K]$
19.35	-0.056	+1.571
37.0	+0.300	-2.705
85.5	+0.082	+4.470

Table 5: Sensitivity of the surface emitted brightness temperature $E_0 T_S$ to real and imaginary part of the dielectric constant at $T = 0^{\circ} C$.

i	b_i
0	-3.64072E-03
1	5.32240E-06
2	1.31797E-05
3	2.47919E-03
4	-3.55719E-05
5	2.96406E-07
6	-6.33305E-03
7	1.69594E-04
8	-8.07822E-05
9	-2.00775E-02
10	1.56056E-04
11	-2.24343E-03
12	1.65838E-04

Table 6: Parameters of the fit (16) for sea water.

REFERENCES

1. Klein, L.A. and C.T. Swift, *An improved model for the dielectric constant of sea water at microwave frequencies.* IEEE J. Oceanic Eng., 1977. **OE-2**: p. 104-111.
2. Debye, P., *Polar Molecules*. Chemical Catalog. 1929, New York.
3. Cole, K.S. and R.H. Cole, *Dispersion and absorption in dielectrics.* J. Chemical Physics, 1941. **9**: p. 341-351.
4. Lane, J.A. and J.A. Saxton, *Dielectric dispersion in pure polar liquids at very high frequencies, III: The effect of electrolytes in solution.* Proc. Roy. Soc, 1952. **A213**: p. 531-545.
5. Ho, W. and W.F. Hall, *Measurements of the dielectric properties of sea water and NaCl solutions at 2.65 GHz,.* J. Geophys. Res., 1973. **78**: p. 6301-6315.
6. Ho, W.W., A.W. Love, and M.J.V. Melle, *Measurements of the dielectric properties of sea water at 1.43 GHz*. 1974, NASA Contractor Report CR-2458.
7. Guillou, C., et al., *Impact of new permittivity measurements on sea surface emissivity modeling in microwaves.* Radio Science, 1998. **33**(3): p. 649 - 667.
8. Wang, J.R., *A comparison of the MIR-Estimated and Model-Calculated Fresh Water Surface Emissivities at 89, 150 and 220 GHz.* IEEE Transactions on Geoscience and Remote Sensing, 2002. **40**(6): p. 1356 - 1365.
9. Wentz, F., *Measurement of Oceanic Wind Vector Using Satellite Microwave Radiometers.* IEEE Transactions on Geoscience and Remote Sensing, 1992. **30**(5): p. 960 - 972.
10. Wentz, F.J., *A Well Calibrated Ocean Algorithm for Special Sensor Microwave/Imager.* Journal of Geophysical Research, 1997. **102**(C4): p. 8703-8718.
11. Wentz, F. and T. Meissner, *AMSR Ocean Algorithm (Version 2)*. 1999, Remote Sensing Systems (http://www.remss.com): Santa Rosa, CA.
12. Liebe, H.J., G.A. Hufford, and T. Manabe, *A model for the complex permittivity of water at frequencies below 1 THz.* International Journal of Infrared and Millimeter Waves, 1991. **12**(7): p. 659 - 675.

13. Stogryn, P.A., et al., *The microwave permittivity of sea and fresh water*. 1995, GenCorp Aerojet: Azusa, CA.

14. Ellison, W., et al., *New permittivity measurements of seawater.* Radio Science, 1998. **33**(3): p. 639 - 648.

15. RSS, R.S.S., *Geophysical Data*. 2002, http://www.remss.com.

16. NCEP, *FNL Analysis*., ftpprd.ncep.noaa.gov Directory: /pub/data/nccf/com/fnl/prod/.

17. Ocean Climate Laboratory, N.O.D.C., *World Ocean Atlas 1998 (WOA98)*. 1999.

18. Stogryn, A., *The apparent temperature of the sea at microwave frequencies.* IEEE Trans. Antennas Propagat., 1967. **AP-15**: p. 278-286.

19. Stogryn, A., *The emissivity of sea foam at microwave frequencies.* J. Geophys. Res., 1972. **77**: p. 1650-1666.

20. Wilheit, T.T., *The effect of wind on the microwave emission from the ocean's surface at 37 GHz.* J. Geophys. Res., 1979. **84**: p. 4921-4926.

21. Wilheit, T.T., *A model for the microwave emissivity of the ocean's surface as a function of wind speed.* IEEE Trans. Gesoci. Electronics, 1979. **GE-17**: p. 244-249.

22. Hollinger, J.P., *Passive microwave measurements of sea surface roughness.* IEEE Trans. Geosci. Electron., 1971. **GE-9**: p. 165-169.

23. Wentz, F., *A two-scale scattering model for foam-free sea microwave brightness temperatures.* Journal of Geophysical Research, 1975. **80**: p. 3441-3446.

24. Sasaki, Y., et al., *The Dependence of Sea-Surface Microwave Emission on Wind Speed, Frequency, Incidence Angle, and Polarization over the Frequency Range From 1 to 40 GHz.* IEEE Transactions on Geoscience and Remote Sensing, 1987. **25**(2): p. 138 - 146.

25. Meissner, T. and F. Wentz, *A Radiative Transfer Model Function for 85.5 GHz SSM/I Ocean Brightness Temperatures.* Radio Science, 2003. **38**(4): p. MAR 31-1 - MAR 31-6.

26. Rosenkranz, P., *Water vapor microwave continuum absorption: A comparison of measurements and models.* Radio Science, 1998. **33**(4): p. 919 - 928.

27. Meissner, T. and F. Wentz, *Radiative Transfer Model Function from SSM/I Brightness*

Temperatures. 2003, Remote Sensing Systems (submitted to AER): Santa Rosa, CA.

28. Rosenkranz, P., *Fortran Code: O2ABS.FOR*. 1998.

29. Liebe, H.J., P.W. Rosenkranz, and G.A. Hufford, *Atmospheric 60-GHz oxygen spectrum: New laboratory measurements and line parameters.* J. Quant. Spectrosc. Radiat. Transfer, 1992. **48**: p. 629 - 643.

30. Schwartz, M.J., *Observation and Modeling of Atmospheric Oxygen Millimeter-wave Transmittance*. 1997, M.I.T.

31. Malmberg, C. and A. Maryott, *Dielectric constant of water from 0° to 100°C.* J. Res. Nat. Bureau of Standards, 1956. **56**: p. 1-8.

32. Archer, D.G. and P. Wang, *The dielectric constant of water and Debye-Huckel limiting law slopes.* J. Phys. Chem. Ref. Data, 1990. **19**: p. 371.

33. Lide, D.R., *Handbook of Chemistry and Physics*. 74 ed. 1993, Ann Arbor: CRC Press. 6-10.

34. Kay, R., G. Vidulich, and K. Pribadi, J. Phys. Chem., 1969. **73**: p. 445.

35. Rusche, E. and W. Good, J. Chem. Phys., 1966. **45**(4667).

36. Angell, C.A., *Supercooled Water*, in *Water: A Comprehensive Treatise*, F. Franks, Editor. 1982, Plenum Press: New York and London.

37. Kaatze, U. and V. Uhlendorf, *The Dielectric Properties of Water at Microwave Frequencies.* Zeitsch f Physik. Chemie Neue Folge, 1981. **126**: p. 151 - 165.

38. Hasted, J.B., et al., *The Temperature Variation of the Near Millimetre Wavelength Optical Constants of Water.* Infrared Phys., 1987. **27**(1): p. 11 - 15.

39. Barthel, J., et al., *A Computer-controlled System of Transmission Lines for the Determination of the Complex Permittivity of Lossy Liquids between 8.5 and 90 GHz.* Ber. Bunsenges. Phys. Chem., 1991. **95**(8): p. 853 - 859.

40. Bertolini, D., M. Cassettari, and G. Salvetti, *The dielectric relaxation time of supercooled water.* J. Chem. Phys., 1982. **76**(6): p. 3285 - 3290.

41. Lipton, A., M. Griffin, and A. Ling, *Microwave Transfer Model Differences in Remote*

Sensing of Cloud Liquid Water at Low Temperatures. IEEE Transactions on Geoscience and Remote Sensing, 1999. **37**(1): p. 620 - 323.

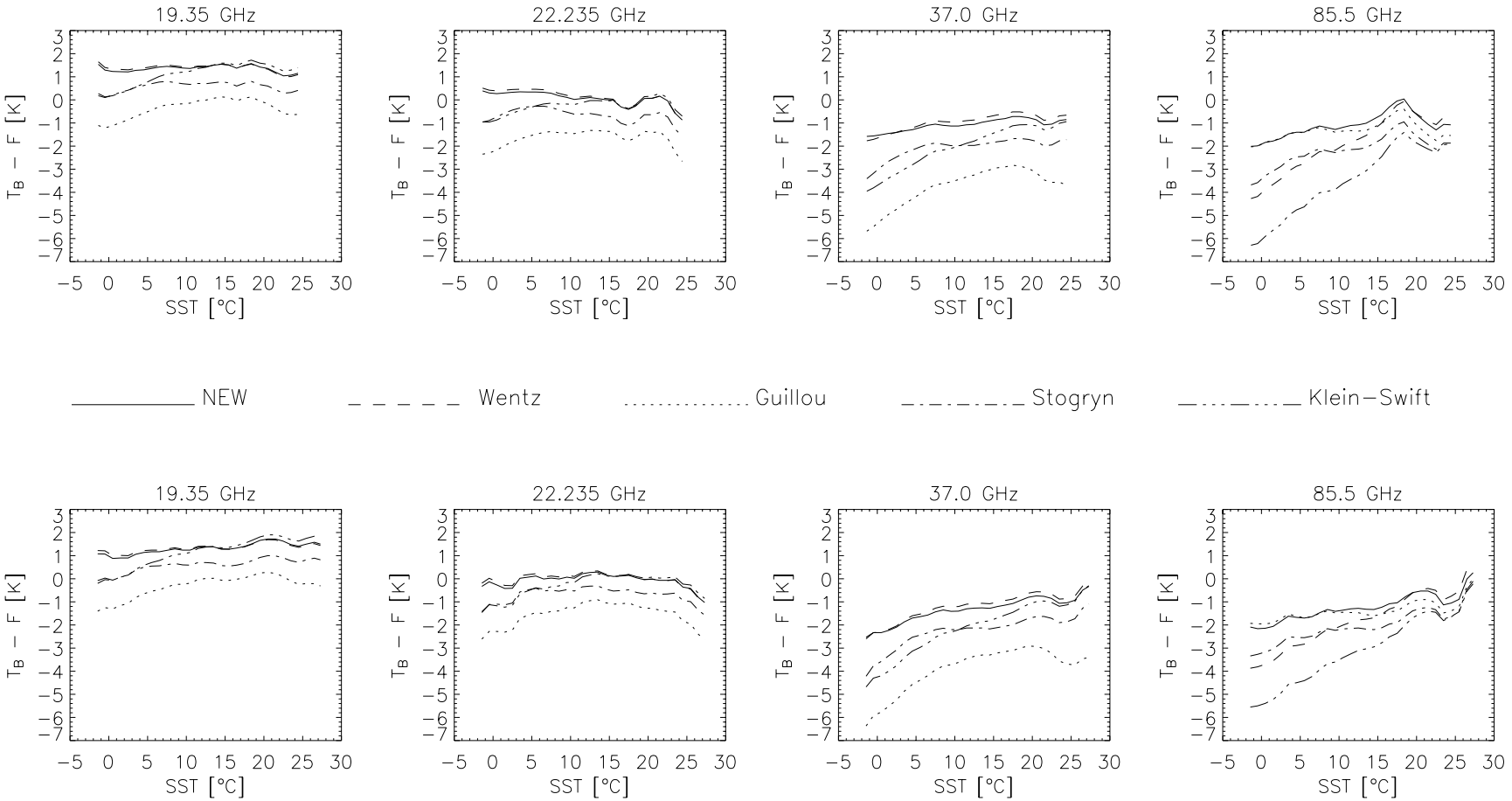
19.35 GHz
22.235 GHz
37.0 GHz
85.5 GHz
T_B − F [K]
SST [°C]
NEW
Wentz
Guillou
Stogryn
Klein−Swift

Figure 1

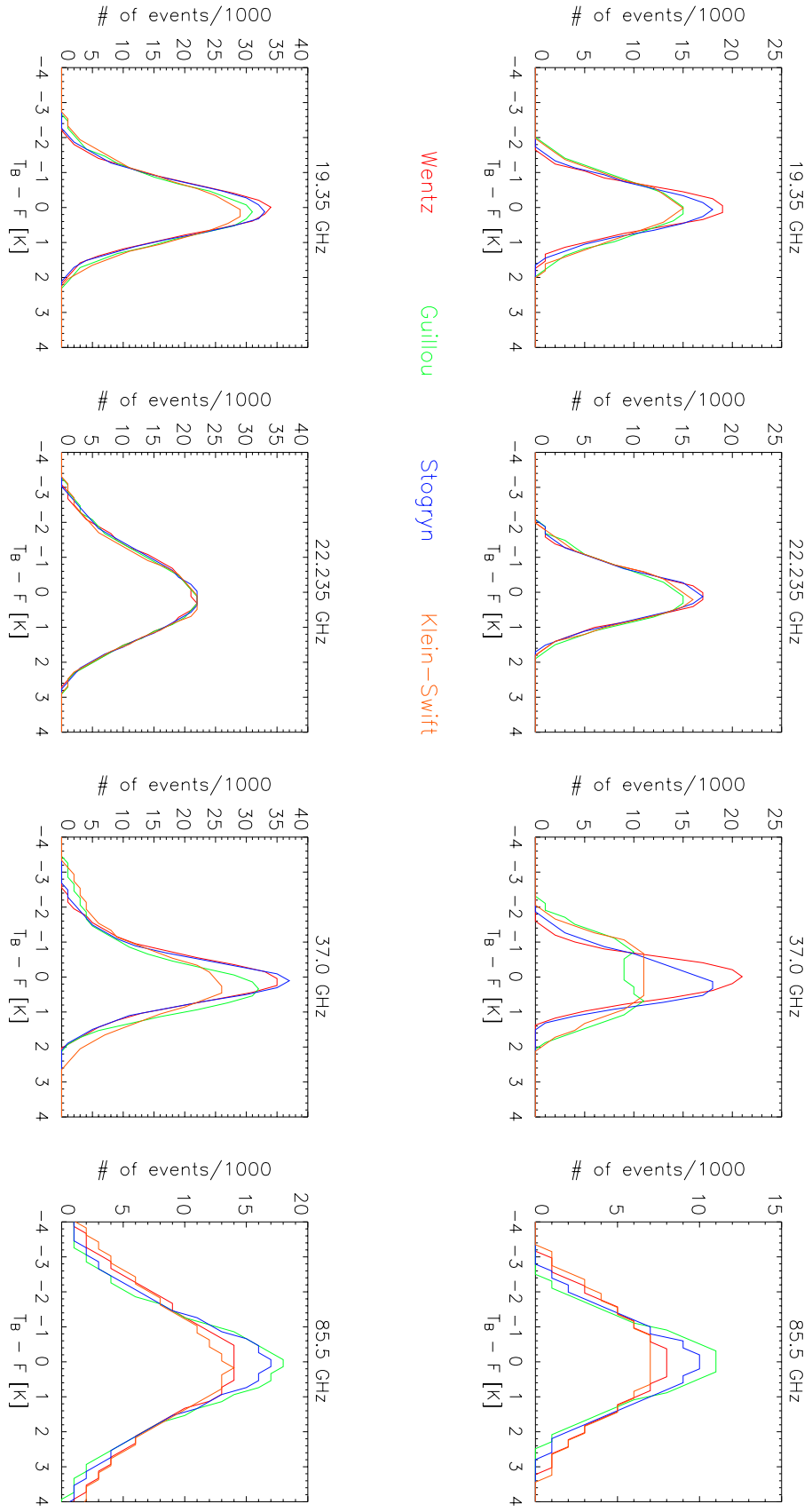
Wentz
Guillou
Stogryn
Klein−Swift
# of events/1000
$T_B - F$ [K]
19.35 GHz
22.235 GHz
37.0 GHz
85.5 GHz

Figure 2

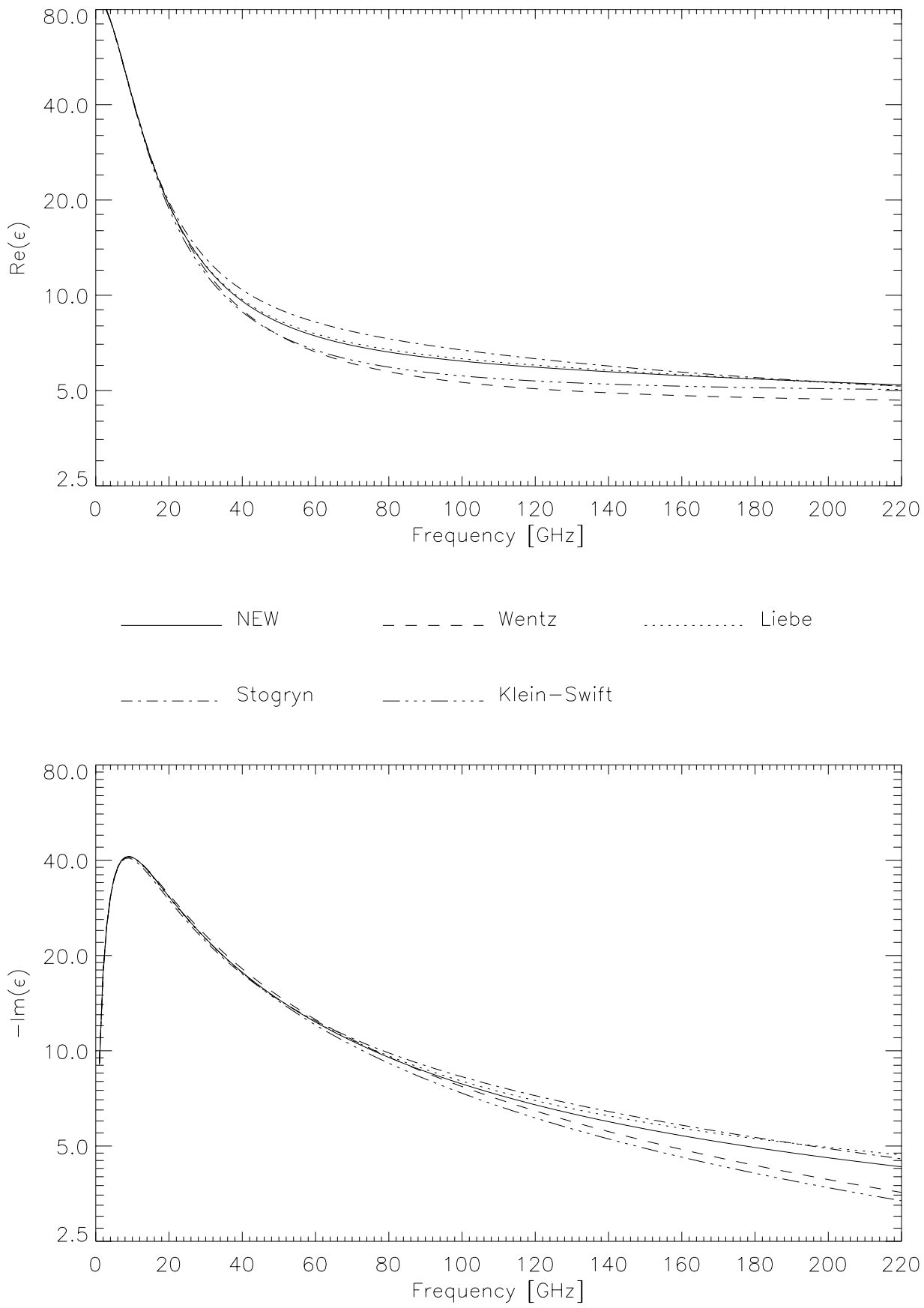
80.0
40.0
20.0
10.0
5.0
2.5
Re(ϵ)
0
20
40
60
80
100
120
140
160
180
200
220
Frequency [GHz]
NEW
Wentz
Liebe
Stogryn
Klein−Swift
80.0
40.0
20.0
10.0
5.0
2.5
−Im(ϵ)
0
20
40
60
80
100
120
140
160
180
200
220
Frequency [GHz]

Figure 3

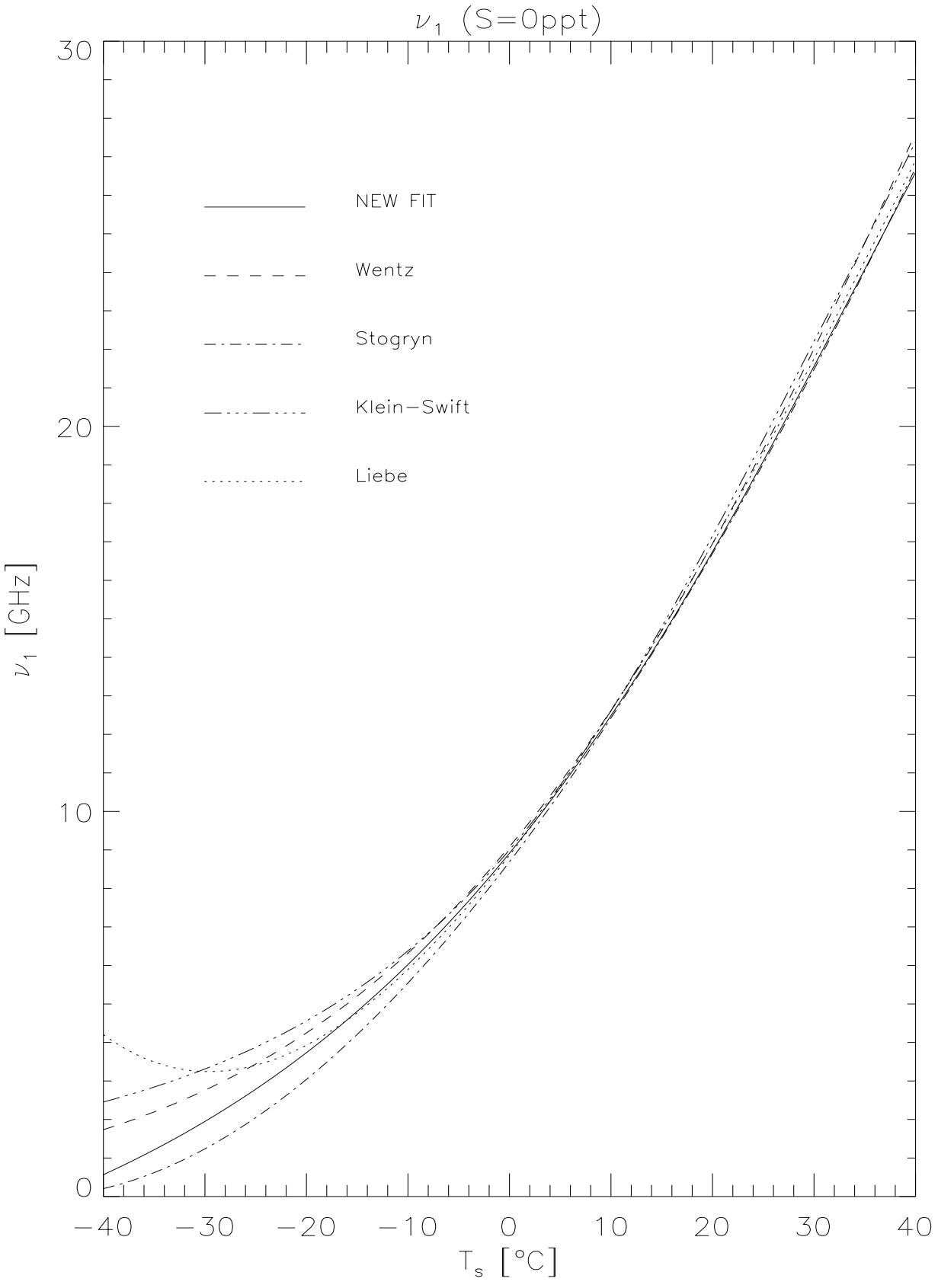
ν_1 (S=0ppt)
30
20
10
0
ν_1 [GHz]
NEW FIT
Wentz
Stogryn
Klein−Swift
Liebe
−40
−30
−20
−10
0
10
20
30
40
T_s [°C]

Figure 4

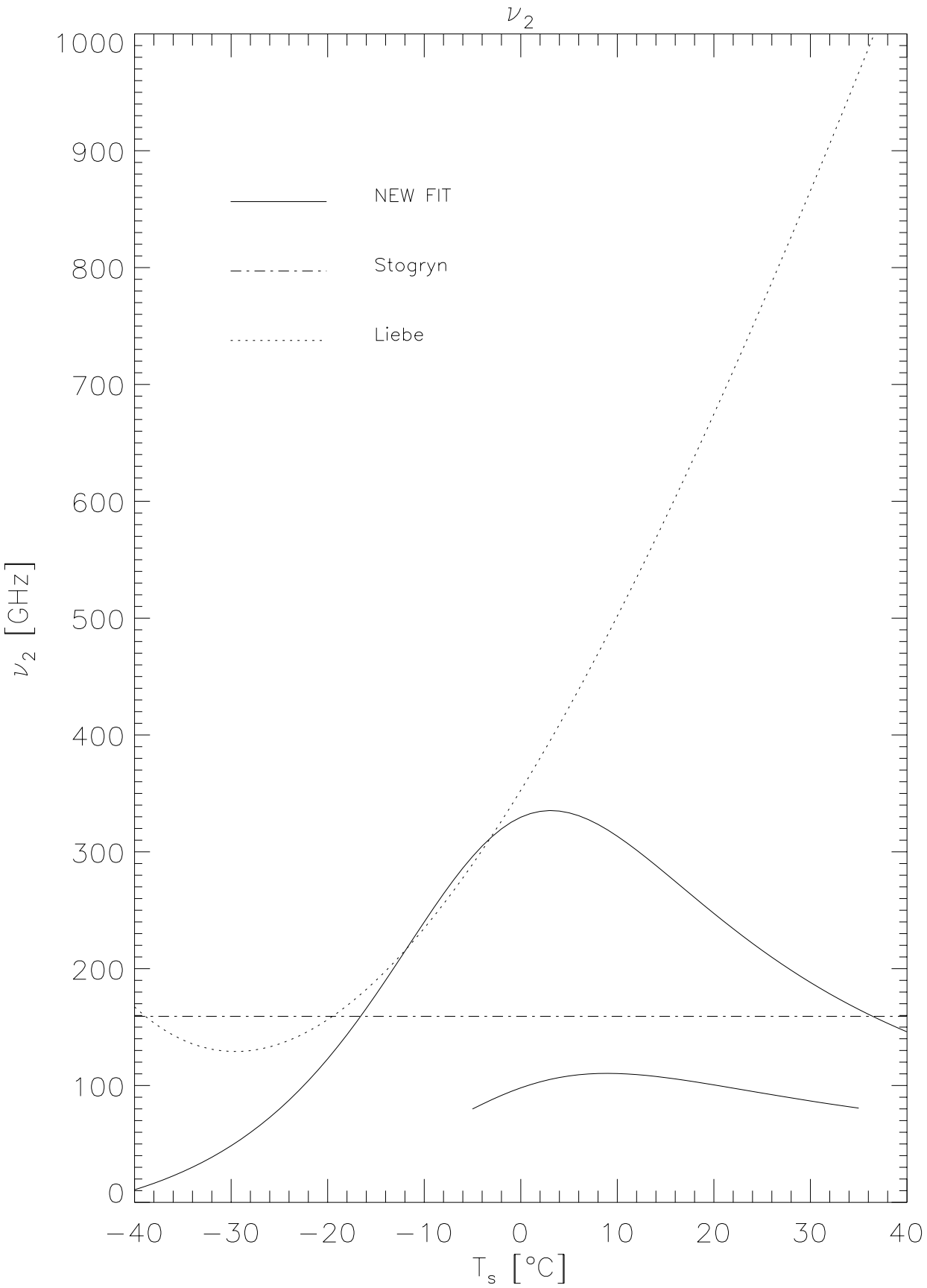
ν_2
1000
900
800
700
600
500
400
300
200
100
0
ν_2 [GHz]
NEW FIT
Stogryn
Liebe
−40
−30
−20
−10
0
10
20
30
40
T_s [°C]

Figure 5

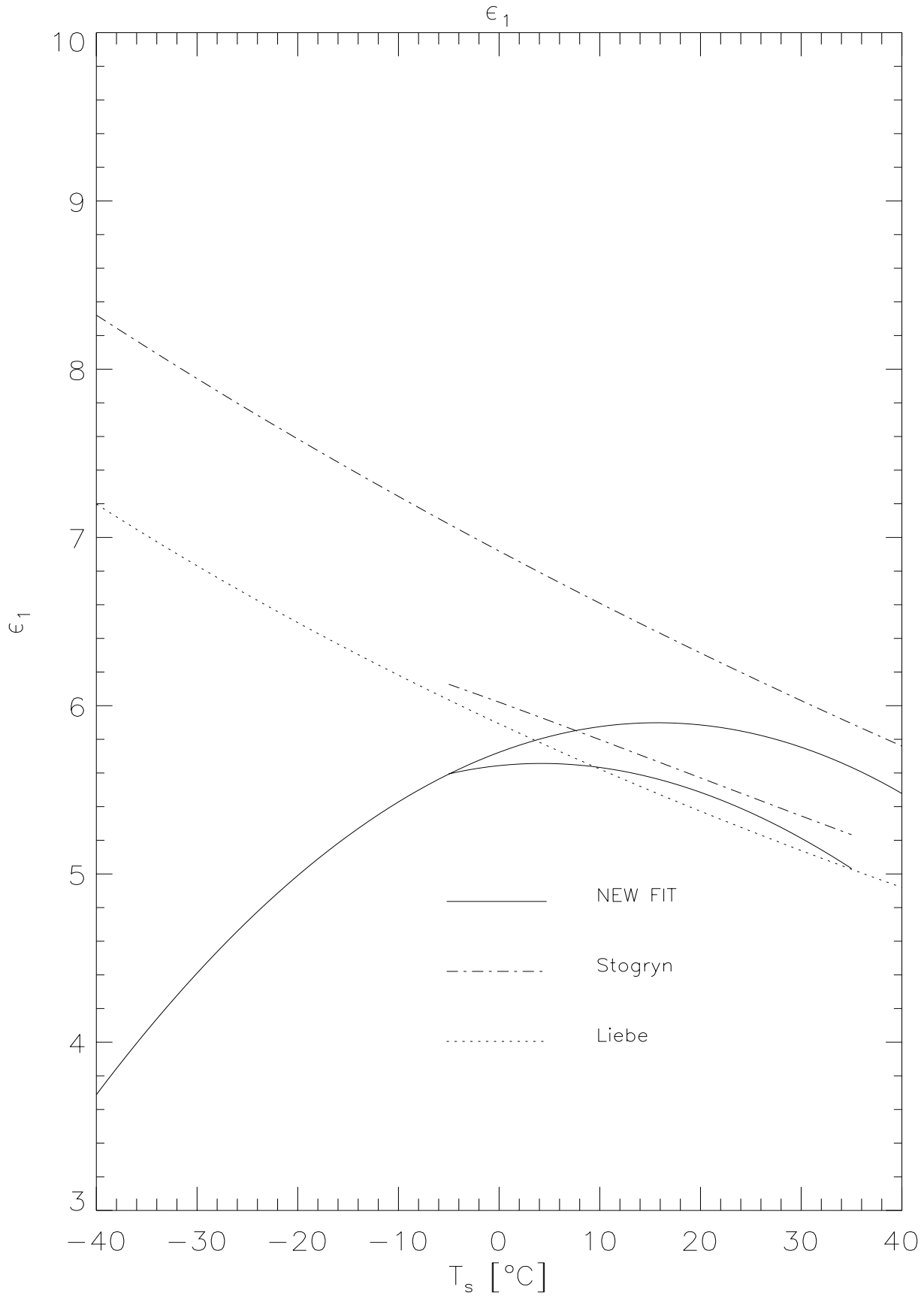
ϵ_1
10
9
8
7
6
5
4
3
ϵ_1
NEW FIT
Stogryn
Liebe
−40
−30
−20
−10
0
10
20
30
40
T_s [°C]

Figure 6

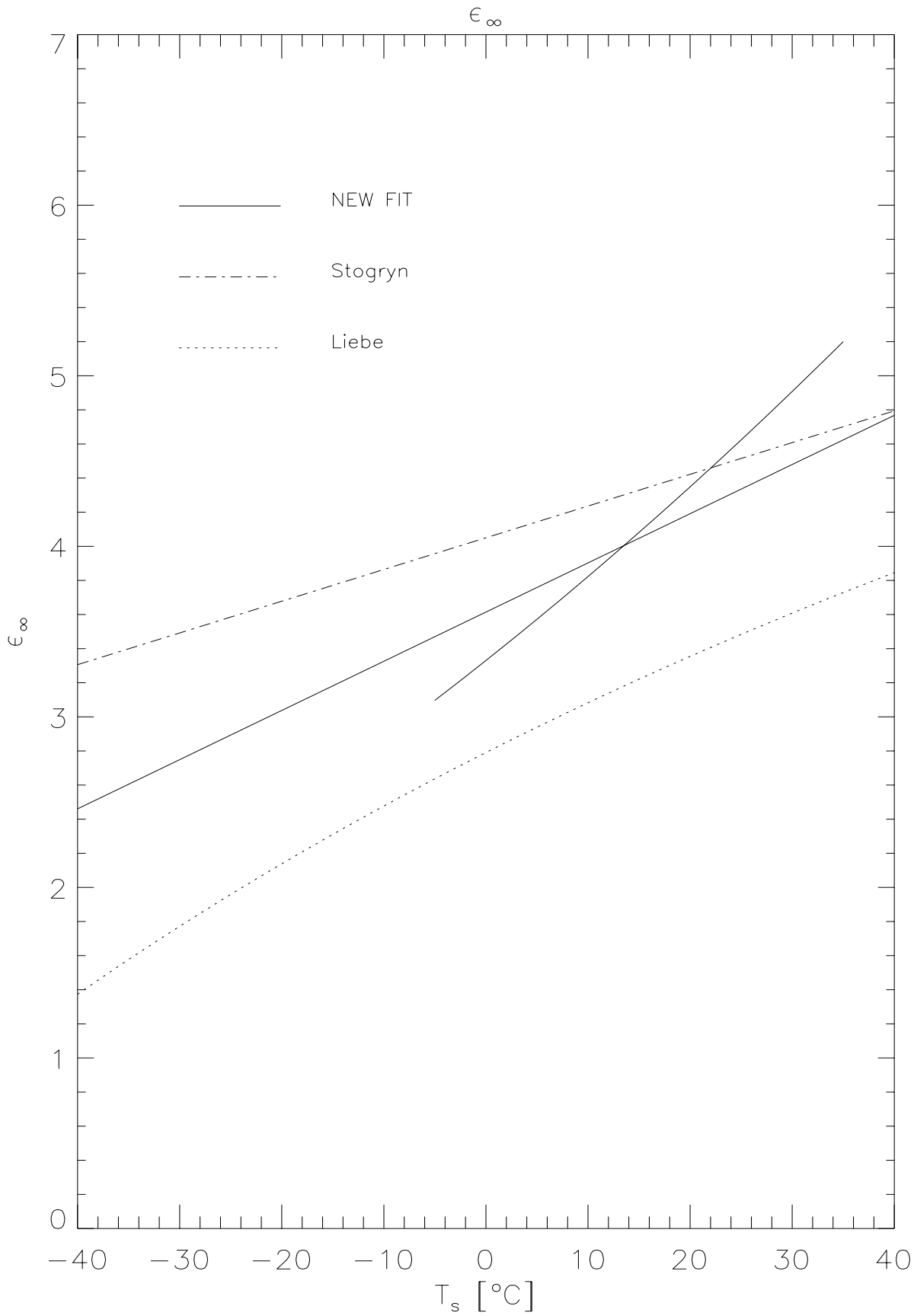
ϵ_∞
NEW FIT
Stogryn
Liebe
ϵ_∞
0
1
2
3
4
5
6
7
−40
−30
−20
−10
0
10
20
30
40
T_s [°C]

Figure 7

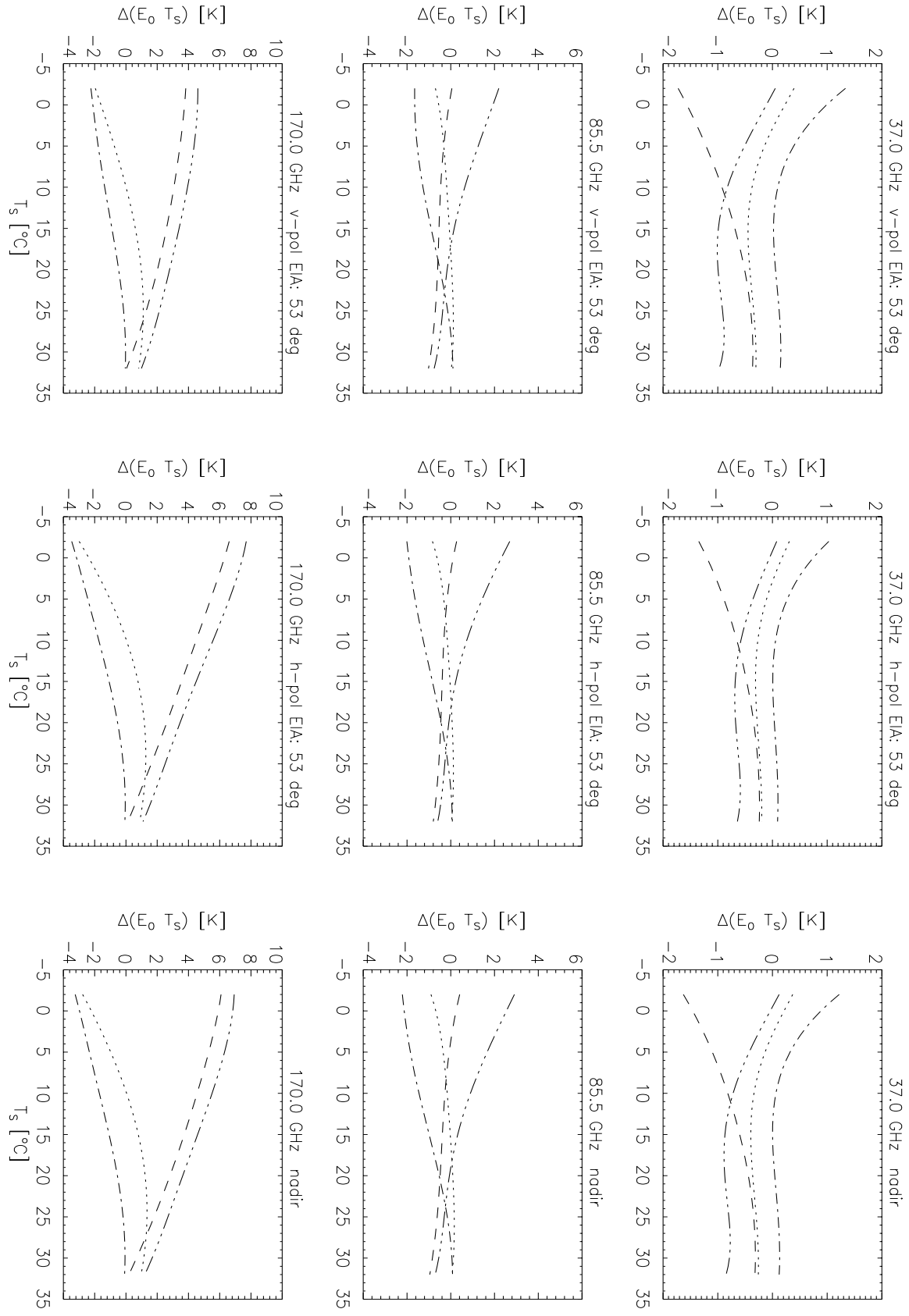
37.0 GHz v-pol EIA: 53 deg
85.5 GHz v-pol EIA: 53 deg
170.0 GHz v-pol EIA: 53 deg
37.0 GHz h-pol EIA: 53 deg
85.5 GHz h-pol EIA: 53 deg
170.0 GHz h-pol EIA: 53 deg
37.0 GHz nadir
85.5 GHz nadir
170.0 GHz nadir
Δ(E0 Ts) [K]
Ts [°C]

Figure 8

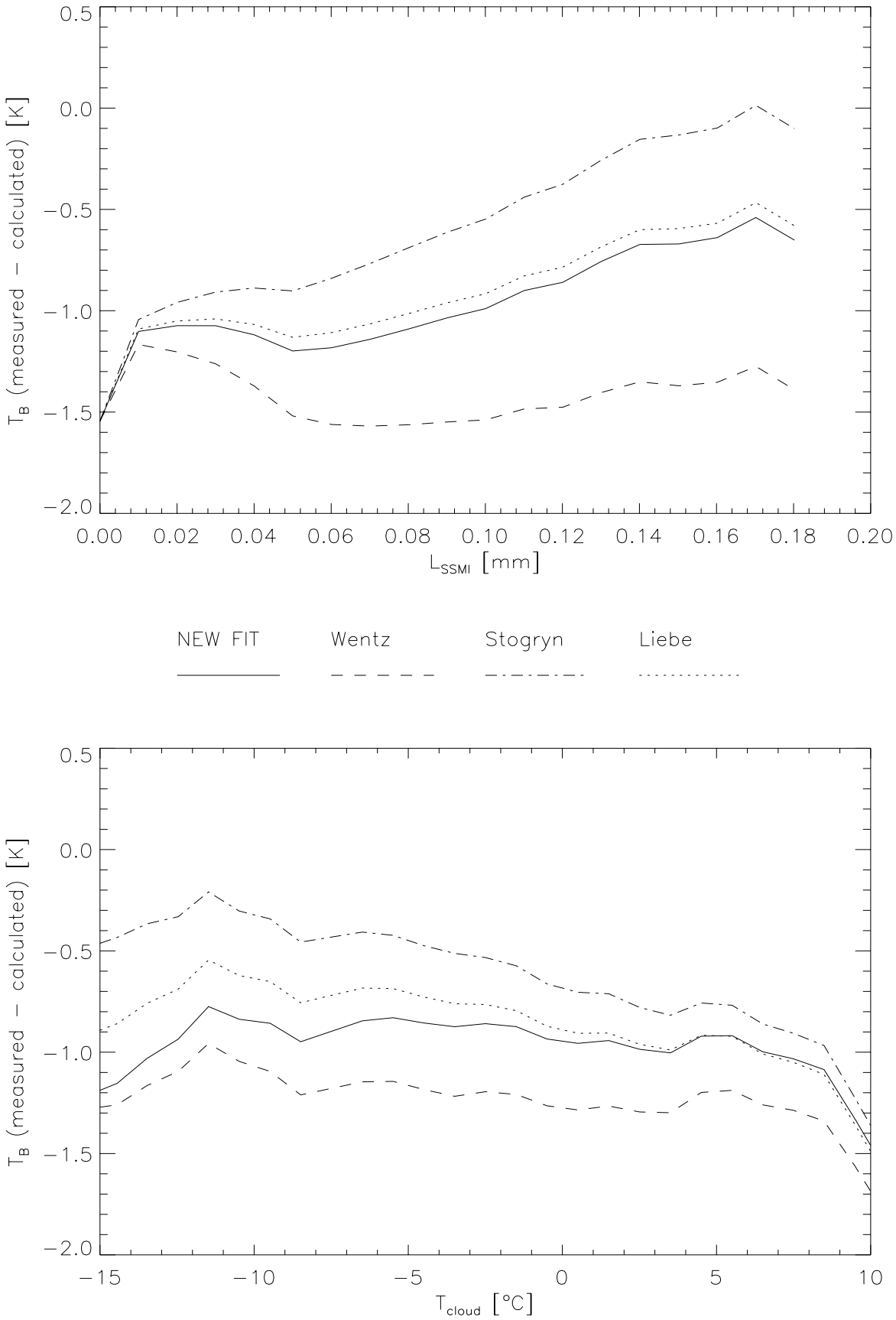
0.5
0.0
−0.5
−1.0
−1.5
−2.0
T_B (measured − calculated) [K]
0.00
0.02
0.04
0.06
0.08
0.10
0.12
0.14
0.16
0.18
0.20
L_{SSMI} [mm]
NEW FIT
Wentz
Stogryn
Liebe
−15
−10
−5
0
5
10
T_{cloud} [°C]

Figure 9

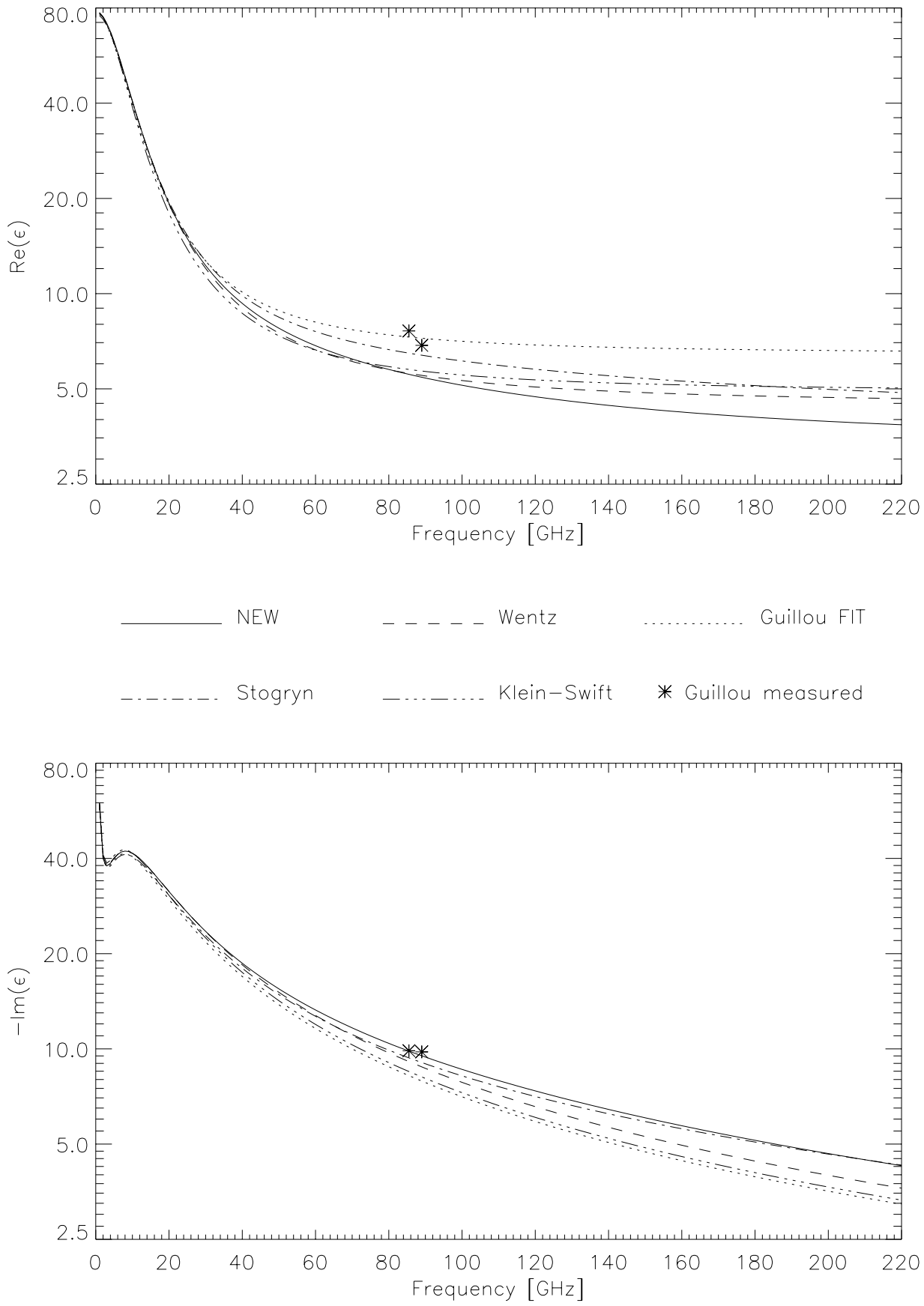
80.0
40.0
20.0
10.0
5.0
2.5
Re(ϵ)
0
20
40
60
80
100
120
140
160
180
200
220
Frequency [GHz]
NEW
Wentz
Guillou FIT
Stogryn
Klein−Swift
Guillou measured
−Im(ϵ)

Figure 10

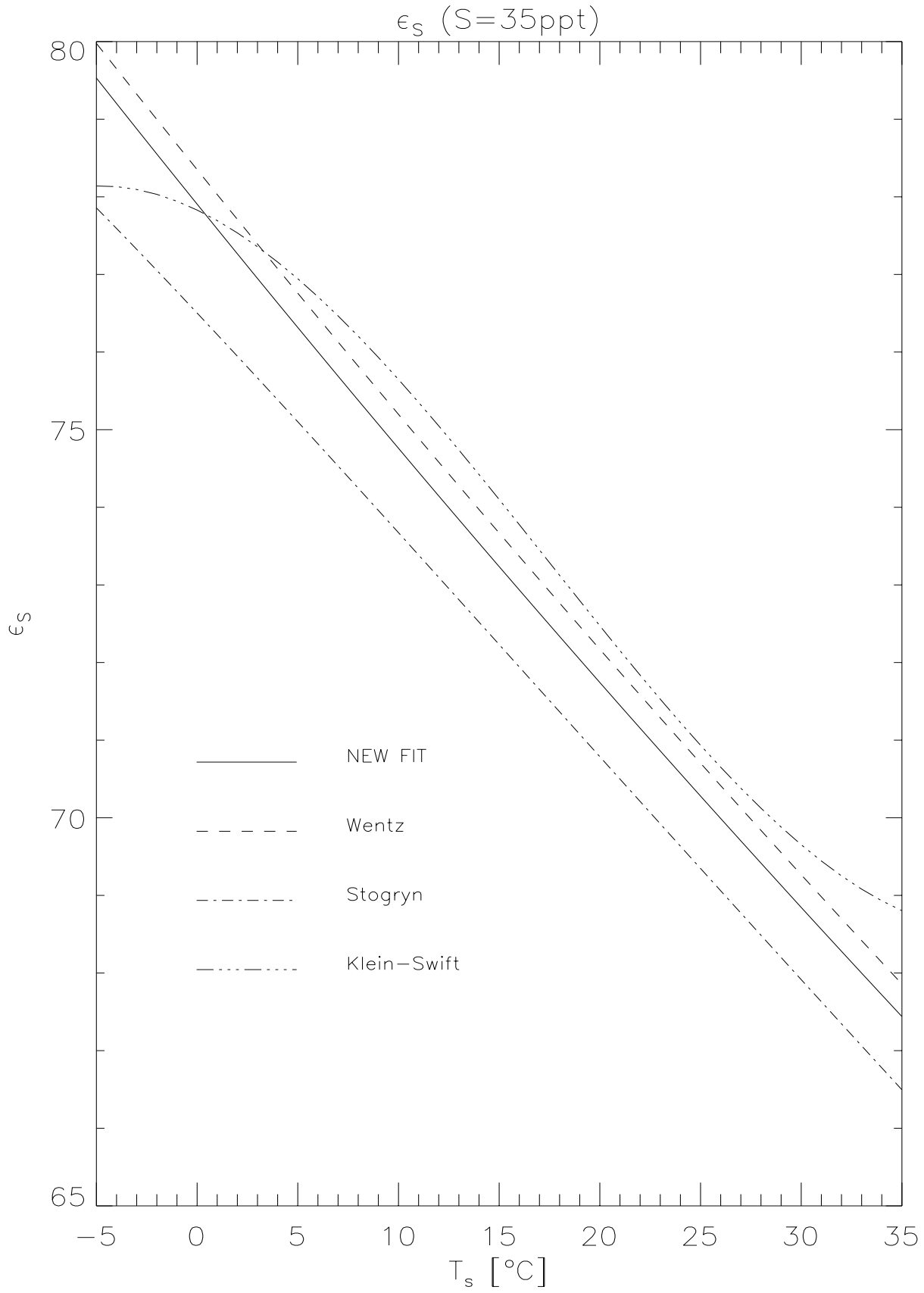
ϵ_S (S=35ppt)
80
75
70
65
ϵ_S
NEW FIT
Wentz
Stogryn
Klein–Swift
−5
0
5
10
15
20
25
30
35
T_s [°C]

Figure 11

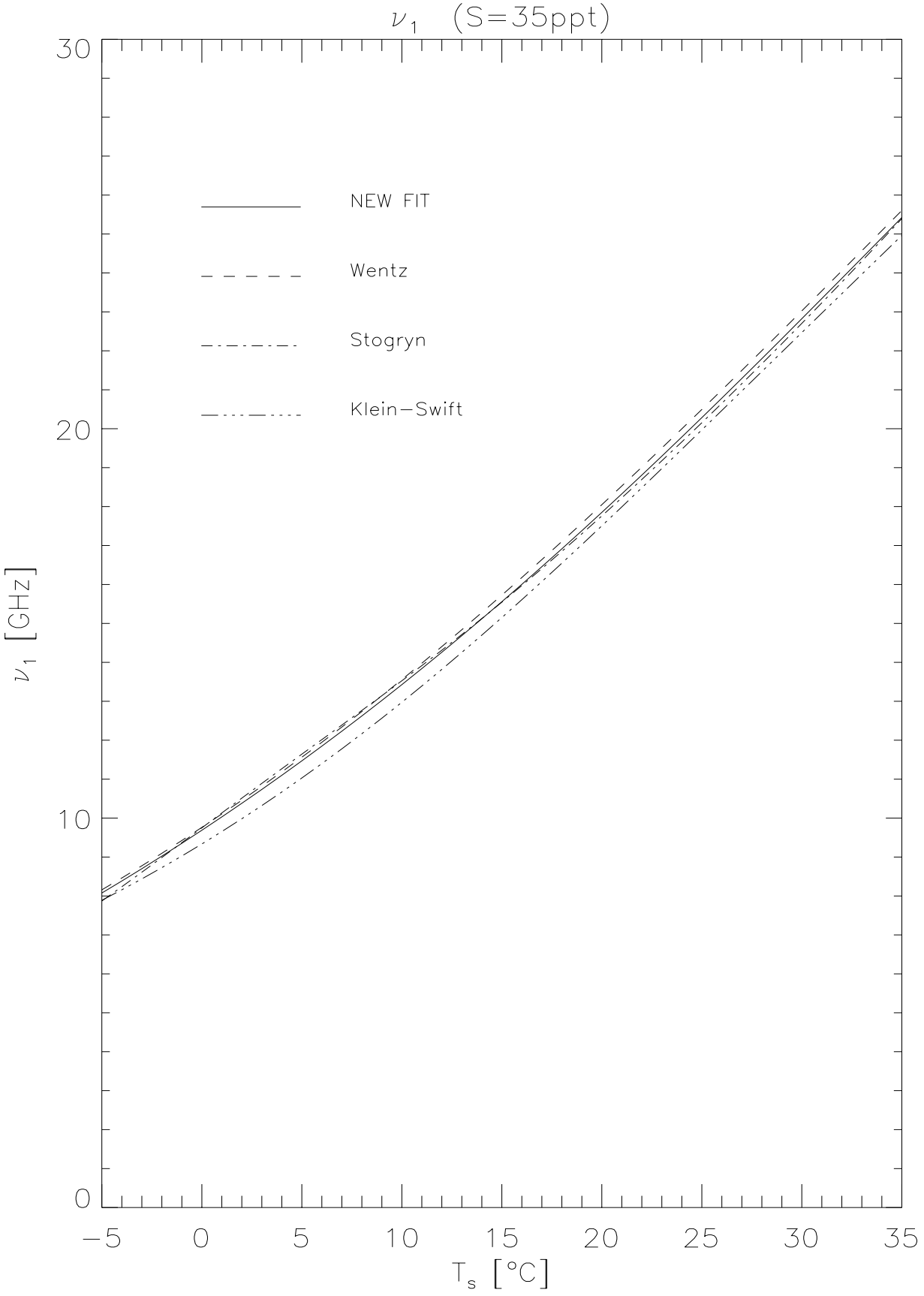
ν_1 (S=35ppt)
NEW FIT
Wentz
Stogryn
Klein–Swift
ν_1 [GHz]
T_s [°C]
30
20
10
0
−5
0
5
10
15
20
25
30
35

Figure 12

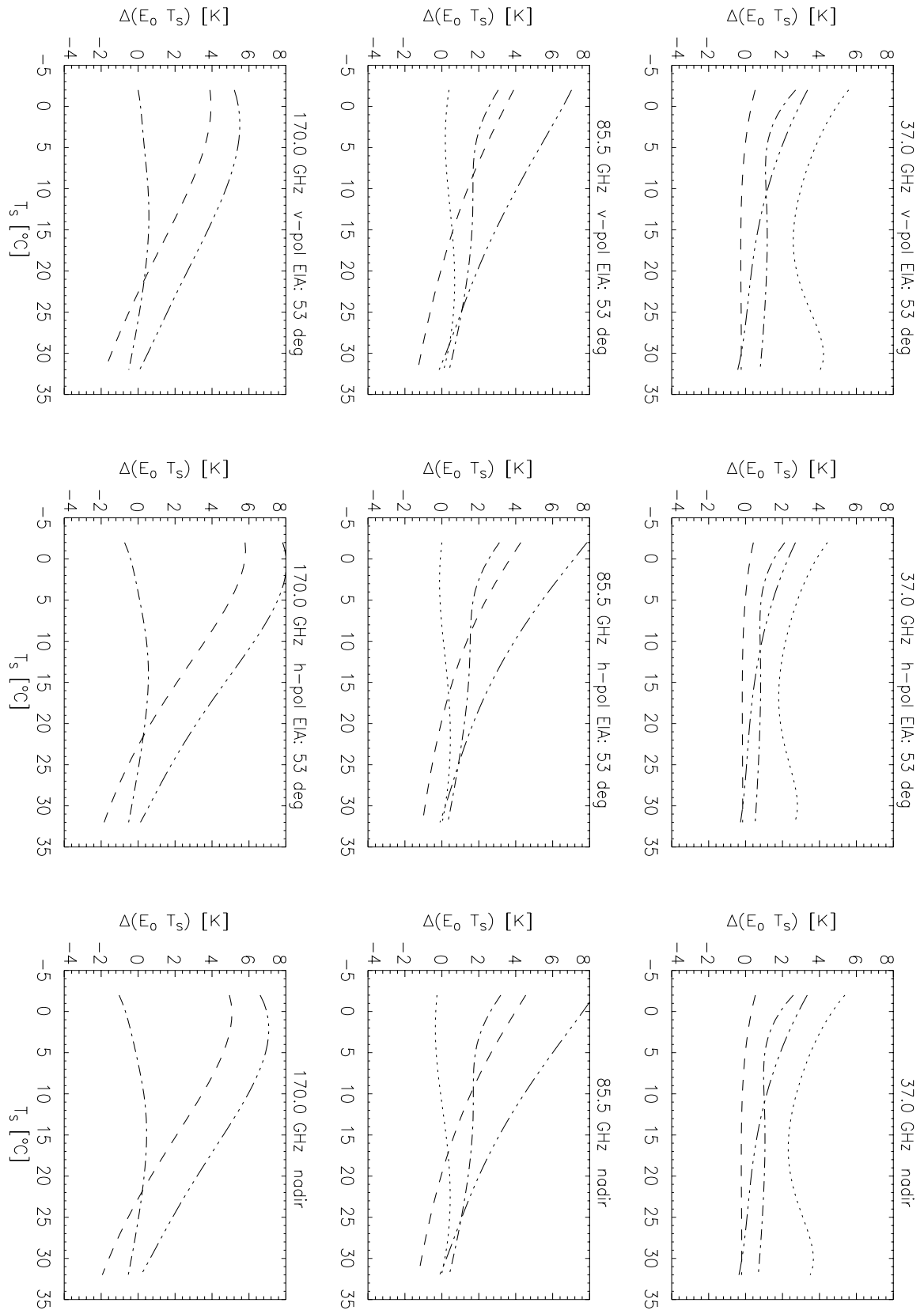
37.0 GHz v-pol EIA: 53 deg
85.5 GHz v-pol EIA: 53 deg
170.0 GHz v-pol EIA: 53 deg
37.0 GHz h-pol EIA: 53 deg
85.5 GHz h-pol EIA: 53 deg
170.0 GHz h-pol EIA: 53 deg
37.0 GHz nadir
85.5 GHz nadir
170.0 GHz nadir
Δ(E0 TS) [K]
TS [°C]

Figure 13